

# Calcium Oscillation Frequency-Sensitive Gene Regulation and Homeostatic Compensation in Pancreatic $\beta$ -Cells

Vehpi Yildirim<sup>1</sup> · Richard Bertram<sup>2</sup>

Received: 25 January 2017 / Accepted: 27 April 2017 / Published online: 11 May 2017  
© Society for Mathematical Biology 2017

**Abstract** Pancreatic islet  $\beta$ -cells are electrically excitable cells that secrete insulin in an oscillatory fashion when the blood glucose concentration is at a stimulatory level. Insulin oscillations are the result of cytosolic  $\text{Ca}^{2+}$  oscillations that accompany bursting electrical activity of  $\beta$ -cells and are physiologically important. ATP-sensitive  $\text{K}^+$  channels (K(ATP) channels) play the key role in setting the overall activity of the cell and in driving bursting, by coupling cell metabolism to the membrane potential. In humans, when there is a defect in K(ATP) channel function,  $\beta$ -cells fail to respond appropriately to changes in the blood glucose level, and electrical and  $\text{Ca}^{2+}$  oscillations are lost. However, mice compensate for K(ATP) channel defects in islet  $\beta$ -cells by employing alternative mechanisms to maintain electrical and  $\text{Ca}^{2+}$  oscillations. In a recent study, we showed that in mice islets in which K(ATP) channels are genetically knocked out another  $\text{K}^+$  current, provided by inward-rectifying  $\text{K}^+$  channels, is increased. With mathematical modeling, we demonstrated that a sufficient upregulation in these channels can account for the paradoxical electrical bursting and  $\text{Ca}^{2+}$  oscillations observed in these  $\beta$ -cells. However, the question of determining the correct level of upregulation that is necessary for this compensation remained unanswered, and this question motivates the current study.  $\text{Ca}^{2+}$  is a well-known regulator of gene expression, and several examples have been shown of genes that are sensitive to the frequency of the  $\text{Ca}^{2+}$  signal. In this mathematical modeling study, we demonstrate that a  $\text{Ca}^{2+}$  oscillation frequency-sensitive gene transcription network can adjust the gene expression level of a compensating  $\text{K}^+$  channel so as to rescue electrical bursting and

---

✉ Richard Bertram  
bertram@math.fsu.edu

<sup>1</sup> Department of Mathematics, Florida State University, Tallahassee, FL 32306, USA

<sup>2</sup> Department of Mathematics and Programs in Molecular Biophysics and Neuroscience, Florida State University, Tallahassee, FL 32306, USA

$\text{Ca}^{2+}$  oscillations in a model  $\beta$ -cell in which the key K(ATP) current is removed. This is done without the prescription of a target  $\text{Ca}^{2+}$  level, but evolves naturally as a consequence of the feedback between the  $\text{Ca}^{2+}$ -dependent enzymes and the cell's electrical activity. More generally, the study indicates how  $\text{Ca}^{2+}$  can provide the link between gene expression and cellular electrical activity that promotes wild-type behavior in a cell following gene knockout.

**Keywords** Gene knockout · Insulin secretion · Pancreatic islets · Bursting · Homeostatic compensation

## 1 Introduction

Pancreatic  $\beta$ -cells are clustered into micro-organs called islets of Langerhans and secrete insulin in response to elevated blood glucose levels. Insulin secretion is typically pulsatile with periods ranging from tens of seconds to a few minutes (Pørksen 2002; Nunemaker et al. 2005; Song et al. 2007; Matveyenko et al. 2008). This pulsatility is due to oscillations in the intracellular  $\text{Ca}^{2+}$  concentration, which are themselves the result of bursting electrical activity of  $\beta$ -cells (Santos et al. 1991; Zhang et al. 2003; Bertram et al. 2010). Insulin pulsatility has been shown to play an important role in glucose homeostasis (Matthews et al. 1983b; Paolisso et al. 1991; Hellman 2009). In a recent study, it was shown that insulin was more effective at reducing blood glucose when presented to the liver in an oscillatory manner (Matveyenko et al. 2012). In type 2 diabetic patients and their near relatives (Matthews et al. 1983a; O'Rahilly et al. 1988; Polonsky et al. 1988), in ob/ob mice (Ravier et al. 2002), and ZDF rats (Sturis et al. 1994), insulin oscillations are impaired. Together, these findings demonstrate the importance of rhythmic insulin secretion for normal blood glucose homeostasis.

Insulin secretion is controlled by interacting metabolic and electrophysiological mechanisms in  $\beta$ -cells. Glucose is taken up by  $\beta$ -cells and metabolized to form ATP, which binds to ATP-sensitive  $\text{K}^+$  channels (K(ATP) channels) in the plasma membrane, putting most of them into an inactive state. The resulting reduction in hyperpolarizing  $\text{K}^+$  current causes membrane depolarization, and the opening of voltage-dependent  $\text{Ca}^{2+}$  ion channels. The increase in intracellular  $\text{Ca}^{2+}$  concentration that results from  $\text{Ca}^{2+}$  influx through these channels evokes exocytosis of insulin-filled granules (Hedekov 1980; Rorsman and Braun 2013). In this process, K(ATP) channels work as molecular sensors of ATP and couple cell metabolism to the membrane potential. There is also evidence that metabolic oscillations act through these channels to drive bursting electrical activity in  $\beta$ -cells (Ren et al. 2013; McKenna et al. 2016; Merrins et al. 2016).

K(ATP) channels are comprised of four inward-rectifying  $\text{K}^+$  channel (Kir6.2) subunits associated with four sulfonylurea receptor (SUR1) subunits [see (Nichols 2006) for review]. A defect in the genes coding these subunits prevents K(ATP) channel expression in the plasma membrane and results in tonic membrane depolarization and persistent hyperinsulinemic hypoglycemia of infancy (PHHI) in humans, a condition caused by excessive insulin secretion (Kane et al. 1996; Shah et al. 2014). However, in genetically engineered SUR1<sup>-/-</sup> mouse islets (SUR1-KO islets), which also do

not express K(ATP) channels in their  $\beta$ -cell plasma membranes, bursting electrical activity and  $\text{Ca}^{2+}$  oscillations persist (Düfer et al. 2004; Nenquin et al. 2004). Furthermore, these mice exhibit nearly normal blood glucose levels unless metabolically stressed (Seghers et al. 2000; Düfer et al. 2004). Clearly, then, there must be some form of compensation to counteract the complete loss of this hyperpolarizing  $\text{K}^+$  current, since otherwise the cells would be tonically active, as they are when K(ATP) channels are blocked with pharmacological agents in wild-type islets (Larsson et al. 1996; Ren et al. 2013). (Whether compensation occurs in PHHI human islets is not presently known.) One study on clonal rat insulinoma RINm5F cells showed that long-term blockade of K(ATP) channels with pharmacological agents, which should result in membrane depolarization and increased  $\text{Ca}^{2+}$  influx, led to increased DNA synthesis (Sjöholm 1995). This study also showed that blocking  $\text{Ca}^{2+}$  influx or inhibiting  $\text{Ca}^{2+}$ -dependent kinases reduces DNA synthesis in these cells. Thus, elevations in the intracellular  $\text{Ca}^{2+}$  concentration in a  $\beta$ -cell clonal cell line may drive compensation through gene transcription. The aim of this paper is to illustrate how this compensation can occur at the right level to maintain the oscillatory activity that is important in glucose homeostasis.

The pattern of activity that an excitable cell, like the  $\beta$ -cell, generates is determined by the type and density of ion channels it expresses in its plasma membrane. Although ion channels are subject to perpetual protein turnover, excitable cells typically maintain a stable phenotype. Studies show that the relation between cellular activity and ion channel expression is bidirectional and the mutual feedback can provide activity-dependent homeostasis in case of a perturbation (Turrigiano et al. 1994; Rosati and McKinnon 2004; Davis 2006; Temporal et al. 2014). When there is a defect in the expression of one type of ion channel, a compensation mechanism can restore homeostasis by regulating the expression of other ion channel types (Xu et al. 2003; Zhou et al. 2003; Rosati and McKinnon 2004). This activity-dependent compensation requires a feedback element that can reflect the electrical activity of the cell and can regulate the expression of ion channels. In excitable cells containing voltage-dependent  $\text{Ca}^{2+}$  channels, the intracellular  $\text{Ca}^{2+}$  concentration reflects the cell's electrical activity. In addition,  $\text{Ca}^{2+}$  is a signaling molecule known to regulate the expression of several proteins including ion channels (Sheng et al. 1991; Barish 1998; Vigmond et al. 2001; West et al. 2001). Computational studies have shown that cytosolic  $\text{Ca}^{2+}$  can indeed be an effective molecule for setting channel expression in such a way that a target electrical activity pattern is achieved (LeMasson et al. 1993; Liu et al. 1998; Olypher and Prinz 2010; O'Leary et al. 2014).

$\text{Ca}^{2+}$  regulates gene expression by transmitting cellular information to the gene transcription network, and theoretical and experimental studies have shown that this information can be encoded in the frequency and amplitude of  $\text{Ca}^{2+}$  oscillations (Dupont and Goldbeter 1998; Li et al. 2012; Smedler and Uhlén 2014). It has been shown that several transcription factors (Dolmetsch et al. 1998; Tsien et al. 1998; Zhu et al. 2008), enzymes (Li et al. 2012) and mitochondrial responses (Hajnoczky et al. 1995; Robb-Gaspers et al. 1998; Collins et al. 2001) are sensitive to the frequency of the  $\text{Ca}^{2+}$  oscillations. In gene transcription networks, it was shown that oscillatory  $\text{Ca}^{2+}$  is more effective in regulating gene expression than constant  $\text{Ca}^{2+}$  (Dolmetsch et al. 1998; Tsien et al. 1998). Furthermore, for some genes, there seems to be an

optimum range of oscillation frequencies in which the signal is most efficient (Tsien et al. 1998; Zhu et al. 2008).

This paper was motivated by the finding that in SUR1-KO mouse islets there is an upregulation of the Kir2.1 isoform of inward-rectifying  $K^+$  channels (manuscript in preparation) and modeling work demonstrating that the resulting Kir2.1 current can effectively compensate for the loss of K(ATP) current and rescue slow bursting oscillations (manuscript submitted). This rescue only occurs, however, if the level of upregulated conductance is right. This raises the question that motivates the current study: How does the cell know the appropriate level of compensation? The most likely answer is that it sets the compensation level so that  $Ca^{2+}$  oscillations with frequency similar to the wild-type cells are restored. But how does it do that? We demonstrate here that a model containing two  $Ca^{2+}$ -dependent enzymes with opposing actions can achieve this. These enzymes effectively decode the frequency of  $Ca^{2+}$  oscillations and regulate the activity of a target transcription factor. By coupling the activity-dependent compensation mechanism with a well-studied  $\beta$ -cell model (Bertram and Sherman 2004), we show that the paradoxical bursting electrical activity, and  $Ca^{2+}$  and insulin oscillations observed in SUR1-KO islets, could result from compensation by another ion channel whose expression is regulated by intracellular  $Ca^{2+}$  dynamics. The optimal expression level of this channel is achieved naturally by the  $Ca^{2+}$ -dependent enzymes. Unlike prior theoretical studies that made use of a target average  $Ca^{2+}$  level to achieve appropriate conductance levels (LeMasson et al. 1993; O'Leary et al. 2014), this mechanism naturally achieves the target activity pattern due to properties of the  $Ca^{2+}$ -dependent enzymes controlling transcription of the compensating channel protein.

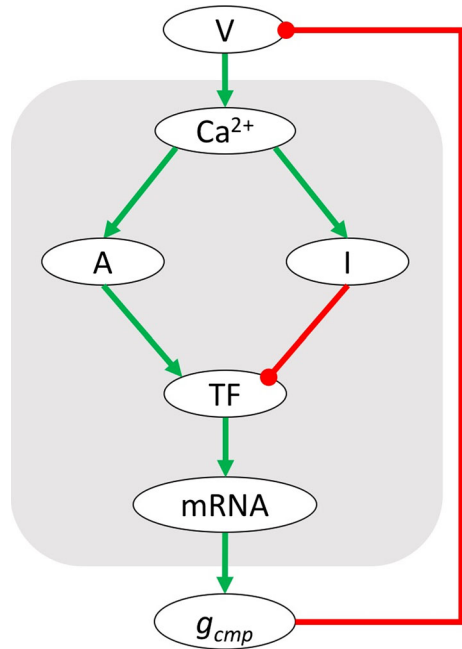
The first part of this paper focuses on how  $Ca^{2+}$ -dependent enzymes can discriminate between  $Ca^{2+}$  signals of different frequencies. It ends by demonstrating that transcription factor activation by two  $Ca^{2+}$ -dependent enzymes with opposing actions can be adjusted to increase monotonically with the frequency of  $Ca^{2+}$  pulse application, or decrease monotonically, or exhibit a bell-shaped response. The second part of the paper combines the transcription model to a model of the activity of the pancreatic  $\beta$ -cell. The  $\beta$ -cell model sets the  $Ca^{2+}$  dynamics that in turn regulate the activity of the transcription factor, thereby closing the loop. This combined model is then used to illustrate the compensation mechanism that is triggered by the removal of the key K(ATP) current. It demonstrates that compensation at the appropriate level to rescue slow  $Ca^{2+}$  oscillations associated with electrical bursting can be achieved through the actions of  $Ca^{2+}$  on two opposing enzymes, provided that the compensating gene product, an ion channel, feeds back onto the membrane potential and contributes to the patterning of electrical activity (Fig. 1).

## 2 Mathematical Model

### 2.1 The Frequency Decoding Model

The  $Ca^{2+}$  frequency decoding network (Fig. 1) consists of a  $Ca^{2+}$ -dependent activator enzyme (A) and an inhibitor enzyme (I), both of which regulate the activity of the target transcription factor. These enzymes could be either kinases or phosphatases,

**Fig. 1** Frequency decoding mechanism is shaded with gray. Green arrows are for stimulatory and red circles are for inhibitory pathways. The model consists of a  $Ca^{2+}$ -dependent activator enzyme (A) and an inhibitor enzyme (I), both of which regulate the activity of the target transcription factor (TF). The activated transcription factor accelerates compensating ion channel mRNA synthesis, which increases the maximal conductance ( $g_{cmp}$ ) of the compensating current. By providing negative feedback on the membrane potential (V),  $g_{cmp}$  completes the feedback loop that underlies activity-dependent homeostasis (Color figure online)



which regulate the activity of proteins by phosphorylating and dephosphorylating them, respectively. Both enzyme families have  $Ca^{2+}$ -dependent members (Rosen et al. 1995), and studies have shown that some  $Ca^{2+}$ -frequency-sensitive transcription factors are activated when phosphorylated (e.g., Oct-1 and NF- $\kappa$ B) (Segil et al. 1991; Oeckinghaus and Ghosh 2009) where others are activated when dephosphorylated (e.g., NFAT) (Rao et al. 1997). Therefore, we avoid using terms kinase and phosphatase and use activator and inhibitor instead. In the model, we assume that the total concentration of the enzymes and the transcription factor do not change over time and we represent the activation of these proteins by the fractions of their active forms. Studies show that  $Ca^{2+}$  binds and activates proteins several  $Ca^{2+}$  dependent enzymes cooperatively (Stemmer and Klee 1994; Bradshaw et al. 2003; Falcke and Malchow 2003; Swulius and Waxham 2013). Taking the nonlinearity induced by positive cooperativity into account, we employ a simple mechanism for enzyme activation kinetics that is easy to analyze and yet encapsulates the kinetic properties of many  $Ca^{2+}$ -dependent enzymes (Falcke and Malchow 2003). The fraction of activator enzyme that is activated by  $Ca^{2+}$ ,  $A_a$ , changes with time according to:

$$\frac{dA_a}{dt} = p_A \frac{c^{n_A}}{c^{n_A} + K_{cA}^{n_A}} (1 - A_a) - d_A A_a \tag{1}$$

where  $p_A$  and  $d_A$  are the activation and deactivation rate constants, respectively. The activation rate is a Hill function of the free intracellular  $Ca^{2+}$  concentration ( $c$ ), with Hill coefficient  $n_A$  and dissociation constant  $K_{cA}$ . The fraction of inhibitor enzyme that is activated by  $Ca^{2+}$ ,  $I_a$ , changes over time according to:

$$\frac{dI_a}{dt} = p_I \frac{c^{n_I}}{c^{n_I} + K_{cI}^{n_I}} (1 - I_a) - d_I I_a. \quad (2)$$

Parameters for the inhibitor enzyme are analogous to those for the activator.

The rate of change of the fraction of activated transcription factor,  $TF_a$ , is given by the difference between its activation and inhibition rates in the following form:

$$\frac{dTF_a}{dt} = A_\infty (1 - TF_a) - I_\infty TF_a. \quad (3)$$

The activation rate of the transcription factor is given by the  $A_a$ -dependent second-order Hill function  $A_\infty$ :

$$A_\infty = \frac{\alpha_A A_a^2}{A_a^2 + K_A^2} \quad (4)$$

where the maximal activation rate is  $\alpha_A$  and  $K_A$  is the value of  $A_a$  for half-maximal activation. The inactivation rate of the transcription factor is given by the  $I_a$ -dependent Hill function  $I_\infty$ :

$$I_\infty = \frac{\beta_I I_a}{I_a + K_I} \quad (5)$$

where  $\beta_I$  is the maximal inhibition rate and  $K_I$  is the  $I_a$  fraction for half-maximal inhibition (we assume a Hill coefficient of 1).

In the initial studies of the  $Ca^{2+}$  frequency decoding mechanism, we simulate changes in the intracellular free  $Ca^{2+}$  concentration with a periodic square wave:

$$c(t) = \begin{cases} c_0 = 0.1, & \text{mod}(t, T) \leq D \\ 0, & \text{mod}(t, T) > D \end{cases} \quad (6)$$

where  $c_0$  is the amplitude of the  $Ca^{2+}$  signal during a pulse,  $T$  is the oscillation period and  $D$  is the pulse duration. Periodic piecewise continuous  $Ca^{2+}$  signals were used in previous experimental (De Koninck and Schulman 1998; Dolmetsch et al. 1998) and computational (Dupont et al. 2003; Schuster et al. 2005; Salazar et al. 2008) studies.  $Ca^{2+}$  signals of this type are easy to manipulate in terms of amplitude and frequency in the experiments and allow derivation of analytical solutions for kinetic equations in computational studies.

## 3 Results

### 3.1 Enzyme Response to a Square-Wave $Ca^{2+}$ Stimulus

Our first goal is to determine the long-term dynamics of an enzyme with  $Ca^{2+}$ -dependent activation described by a Hill function. This enzyme could either activate or repress a gene transcription factor. As described in Methods with Eqs. 1–2, the form we use is:

$$\frac{dE_a}{dt} = p_E \frac{c^{n_E}}{c^{n_E} + K_E^{n_E}} (1 - E_a) - d_E E_a \quad (7)$$

where  $E_a$  is the fraction of an enzyme that is in its activated state. Assuming that all enzyme molecules are initially in an inactive form and that the enzyme is subject to a periodic square-wave  $Ca^{2+}$  signal (Eq. 6), we can derive an analytical solution to Eq. 7 during periods where the  $Ca^{2+}$  input is on (top) or off (bottom):

$$E_a(t) = \begin{cases} E_{ss} \left( 1 - e^{-(p_E^* + d_E)t} \right), & t < D \\ E_a(D) e^{-d_E t}, & D \leq t \leq T \end{cases}, \tag{8}$$

where

$$p_E^* = p_E \frac{c_0^{n_E}}{c_0^{n_E} + K_E^{n_E}} \tag{9}$$

is the  $Ca^{2+}$ -dependent activation rate of the enzyme, and

$$E_{ss} = \frac{1}{1 + \frac{d_E}{p_E^*}} \tag{10}$$

is the steady-state fraction of activated enzyme with  $Ca^{2+}$  concentration  $c_0$ . Equation 8 shows that the characteristic response time of the enzyme to the stimulus is  $1/d_E$ . Thus, if  $d_E$  is large, then the response time is fast and  $E_{ss}$  is small. In this case, the activated enzyme concentration closely follows the  $c$  time course. However, many enzymes respond to a stimulus slowly due to the conformational changes and/or phosphorylation necessary for their activation (Frieden 1970, 1979). The rate-limiting slow activation dynamics serve as a low-pass filter against noise in the input and also enable the enzyme to have an optimal response to certain stimulus frequencies (Wu and Xing 2012). Our aim is to construct a signaling model that will exhibit such a response to the periodic  $Ca^{2+}$  stimulus, so we tune  $d_E$  and  $p_E$  so that the characteristic response time of the enzyme is comparable to the period of the square-wave  $Ca^{2+}$  stimulus.

Figure 2 shows one period of a representative  $Ca^{2+}$  stimulus (inset, red) and the resulting activated enzyme time course (black solid) over many periods of the stimulus. The time-varying mean value of the fraction of activated enzyme over the  $i$ th stimulus cycle  $\bar{E}_{a,i}$  is:

$$\bar{E}_{a,i} = \frac{1}{T} \int_{iT}^{(i+1)T} E_a(t) dt \tag{11}$$

and is shown by the dashed curve in the figure. This eventually settles to a value  $\bar{E}_a$ . The formula for this steady-state mean activated enzyme fraction is derived in ‘‘Appendix 1’’ and is given by:

$$\bar{E}_a = E_{ss} \left( \frac{D}{T} + \frac{E_{ss}}{d_E T} \frac{\left( 1 - e^{-D(p_E^* + d_E)} \right) \left( 1 - e^{-d_E(T-D)} \right)}{1 - e^{-(p_E^* D + d_E T)}} \right). \tag{12}$$

This provides a manageable expression for  $\bar{E}_a$  in terms of the  $Ca^{2+}$  pulse duration ( $D$ ) and the period ( $T$ ) of the periodic square-wave  $Ca^{2+}$  stimulus.

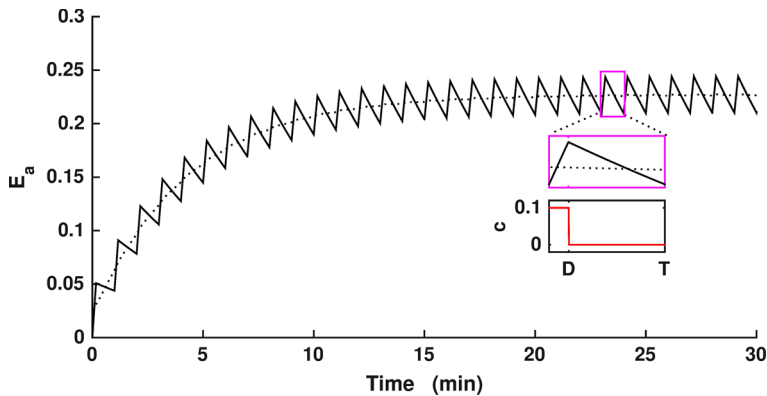


**Fig. 2** Time course of the fraction of the activated enzyme (*black solid curve*) with a representative square-wave  $\text{Ca}^{2+}$  signal (*red curve, inset*). The enzyme integrates the  $\text{Ca}^{2+}$  signal over time. The mean fraction of activated enzyme (*black dotted curve*) initially increases and reaches an equilibrium once the activated enzyme level becomes periodic (Color figure online)

### 3.2 Oscillations are More Effective than Constant $\text{Ca}^{2+}$ at Low Frequencies When $\text{Ca}^{2+}$ Binds to an Enzyme Cooperatively

Is  $\text{Ca}^{2+}$  more effective at activating an enzyme when it is delivered as periodic square pulses? To answer this question, we compare the long-term activated enzyme level with a square-wave stimulus to that obtained with a constant stimulus of the same mean value of  $\text{Ca}^{2+}$ . This value,  $c_c$ , is:

$$c_c = c_0 \frac{D}{T}. \quad (13)$$

Substituting  $c_c$  for  $c$  in the equilibrium activated enzyme function Eq. 10 yields, after some algebra,

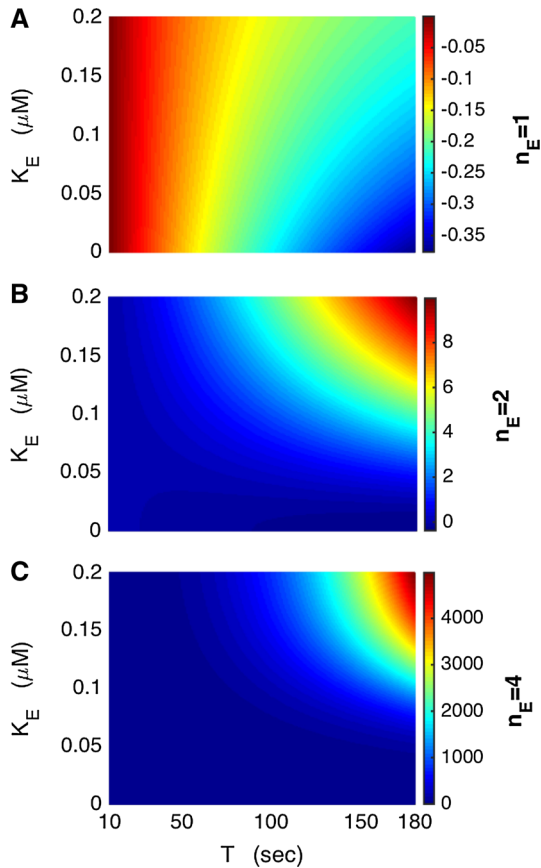
$$\bar{E}_{a,c} = \frac{1}{1 + \frac{d_E}{P_E} \left( 1 + \left( \frac{K_E}{c_c} \right)^{n_E} \right)} \quad (14)$$

which gives the steady-state fraction of the activated enzyme with constant  $\text{Ca}^{2+}$ . We now compare  $\bar{E}_{a,c}$  with the long-term average activated enzyme level with a square-wave stimulus,  $\bar{E}_a$ , using what we call the ‘Oscillation Efficiency’:

$$\text{Oscillation Efficiency} = \frac{\bar{E}_a - \bar{E}_{a,c}}{\bar{E}_{a,c}}. \quad (15)$$

Figure 3 shows the oscillation efficiency over a range of values of the oscillation period  $T$  and the  $\text{Ca}^{2+}$  dissociation constant for the enzyme,  $K_E$ , using three different levels of cooperativity  $n_E$ . In each case,  $D = 10$  s. When  $T \rightarrow D$  in Eqs. 12 and 14, both  $\bar{E}_a \rightarrow E_{ss}$  and  $\bar{E}_{a,c} \rightarrow E_{ss}$ , and consequently, the oscillation efficiency approaches zero independent of  $n_E$ . That is, the responses of the enzyme to the square wave and

**Fig. 3** Cooperativity increases the oscillation efficiency (Eq. 15) at low frequencies when  $\text{Ca}^{2+}$  binds to enzyme with low affinity (larger  $K_E$ ). **a** When  $n_E = 1$ , the oscillation efficiency is negative for all  $K_E$  values, indicating that a constant  $\text{Ca}^{2+}$  stimulus is more effective than a square-wave stimulus. **b, c** With increasing  $\text{Ca}^{2+}$  binding cooperativity, the square-wave  $\text{Ca}^{2+}$  stimulus becomes more effective, particularly at low frequencies (Color figure online)



constant stimuli are similar when there is little time between stimuli, regardless of the cooperativity (leftmost portions of each panel in Fig. 3).

Figure 3a shows that when  $n_E = 1$ , oscillation efficiency is negative ( $\bar{E}_a \leq \bar{E}_{a,c}$ ) for all values of  $K_E$  shown. That is, when  $\text{Ca}^{2+}$  binds to the enzyme non-cooperatively, a constant  $\text{Ca}^{2+}$  stimulus is more effective than a square-wave  $\text{Ca}^{2+}$  stimulus. However, with positive cooperativity ( $n_E > 1$ ), the oscillation efficiency increases with longer periods  $T$  and larger values of  $K_E$  ( $\frac{d\bar{E}_a}{dT} > \frac{d\bar{E}_{a,c}}{dT}$ ) due to the exponential dependence of  $\bar{E}_{a,c}$  on  $n_E$ . Thus, the periodic square wave  $\text{Ca}^{2+}$  becomes more effective at activating the enzyme than constant  $\text{Ca}^{2+}$  at lower frequencies (Fig. 3b, c). Since  $K_E$  is divided by  $c_c$  and thus multiplies  $T$  in Eq. 14, when  $K_E$  is small,  $T$  must be large for this effect to be seen (the efficiency is highest in the upper right portions of panels B and C).

How does  $\text{Ca}^{2+}$  cooperativity affect the activated enzyme level? This depends on whether  $\text{Ca}^{2+}$  is constant or delivered as periodic square pulses. For the case of a constant  $\text{Ca}^{2+}$  stimulation, this is simple; Eq. 14 shows that if  $c_c > K_E$ , then cooperativity increases the activated enzyme level, while if  $c_c < K_E$ , it decreases it. If the  $\text{Ca}^{2+}$  signal is a periodic square wave, then the influence of cooperativity on the long-term mean activated enzyme concentration,  $\bar{E}_a$  (Eq. 12), is determined by

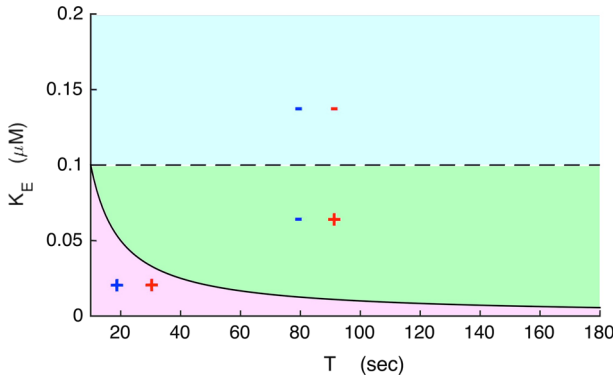


**Fig. 4** The  $K_E$  values where cooperative  $\text{Ca}^{2+}$  binding enhances or reduces the enzyme activation are indicated by + or -, respectively. *Blue symbols* are for a constant  $\text{Ca}^{2+}$  stimulus, and *red symbols* are for a square-wave stimulus with the same mean level. The *solid curve* satisfies  $K_E = c_0 \frac{D}{T} = c_c$ , while the *dashed line* satisfies  $K_E = c_0$ . Oscillations increase the range of the parameter space where cooperativity has a positive impact on the enzyme activation (Color figure online)

$$\frac{d\bar{E}_a}{dn_E} = \frac{d\bar{E}_a}{dp_E^*} \frac{dp_E^*}{dn_E}. \tag{16}$$

It can be shown that  $\frac{d\bar{E}_a}{dp_E^*} > 0$  and,

$$\frac{dp_E^*}{dn_E} = \frac{c_0^{n_E} K_E^{n_E} \left( \ln \frac{c_0}{K_E} \right)}{\left( c_0^{n_E} + K_E^{n_E} \right)^2} \tag{17}$$

which is positive if the argument of the natural log is greater than 1, so  $\frac{d\bar{E}_a}{dn_E} > 0$  if  $K_E < c_0$ . Therefore, for a periodic square-wave  $\text{Ca}^{2+}$  signal,  $\text{Ca}^{2+}$  cooperativity increases the activated enzyme level if the amplitude of the  $\text{Ca}^{2+}$  pulse is greater than the dissociation constant, else it decreases the activated enzyme level.

The cooperativity effects are illustrated in Fig. 4. Below the curve  $K_E = c_0 \frac{D}{T}$  (Fig. 4, purple region), cooperativity increases activated enzyme if the  $\text{Ca}^{2+}$  level is constant (Fig. 4, blue +). Below the dashed line  $K_E = c_0$  (Fig. 4, purple and green regions) cooperativity increases activated enzyme if the  $\text{Ca}^{2+}$  level is a square wave (Fig. 4, red +). Since the latter area is larger, the range of  $K_E$  values where cooperativity increases the activated enzyme level is greater with a square-wave  $\text{Ca}^{2+}$  stimulus than with a constant stimulus with the same average  $\text{Ca}^{2+}$  level.

### 3.3 Frequency Decoding Capability of the Enzyme Increases with Its Affinity to $\text{Ca}^{2+}$

It is clear that the activated enzyme level increases with the frequency of the square wave  $\text{Ca}^{2+}$ . However, it is ambiguous whether increased activation is due to the

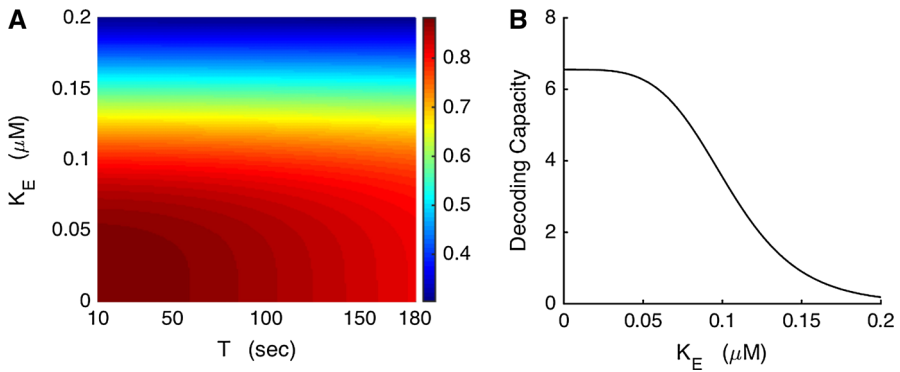


**Fig. 5** The enzyme is capable of decoding the  $\text{Ca}^{2+}$  oscillation frequency when the average  $\text{Ca}^{2+}$  is held constant. In Eq. 12, we set  $D = \gamma T$  and  $\gamma = 0.25$ . **a** Fraction of activated enzyme is color coded with *dark red* being the highest and *dark blue* being the lowest values. Enzyme activation is higher when short square-wave  $\text{Ca}^{2+}$  pulses are separated by short intervals. **b** Frequency decoding capacity of the enzyme declines as  $K_E$  increases. The decoding capacity is defined in Eq. 18 (Color figure online)

increased average  $\text{Ca}^{2+}$  concentration with frequency or due to the increased frequency itself. To what extent is the activation responding to the frequency of the oscillations? To answer this question, it is necessary to fix the average  $\text{Ca}^{2+}$  as the oscillation frequency is varied. We do this while keeping the duty cycle,  $\gamma = \frac{D}{T}$ , fixed. Consequently, as  $T$  is varied, the average  $\text{Ca}^{2+}$  remains constant. Figure 5 shows the fraction of activated enzyme as  $T$  and  $K_E$  are varied, with  $\gamma = 0.25$  and  $n_E = 4$ . For all  $K_E$  values, the activated enzyme concentration decreases with the period of the square wave (Fig. 5a), so short  $\text{Ca}^{2+}$  pulses separated by small intervals are more effective at activating the enzyme. How does the frequency decoding capability of the enzyme depend on its affinity to  $\text{Ca}^{2+}$ ? To find out, for each  $K_E$  value, we calculate the fraction of activated enzyme obtained for a short-period stimulus,  $T = 10$  s, and a long-period stimulus,  $T = 180$  s. We denote these by  $\bar{E}_{a,10}(K_E)$  and  $\bar{E}_{a,180}(K_E)$ , respectively. The effect of frequency for each  $K_E$  value is reflected in the difference between these two. Normalizing this with respect to  $\bar{E}_{a,180}(K_E)$  yields the following  $K_E$ -dependent estimate for the ‘Decoding Capacity’ of the enzyme:

$$\text{Decoding Capacity} = 100 \cdot \frac{\bar{E}_{a,10}(K_E) - \bar{E}_{a,180}(K_E)}{\bar{E}_{a,180}(K_E)}. \tag{18}$$

The frequency decoding capacity of the enzyme decreases as  $K_E$  increases (Fig. 5b). Thus, enzymes with higher  $\text{Ca}^{2+}$  affinity are better able to decode the frequency of oscillations.

### 3.4 Opposing Actions of the Activator and Inhibitor Enzymes Determine the Frequency Response Regime of the Transcription Factor

In this section, we investigate the frequency-dependent regulation dynamics of the transcription factor, subject to  $\text{Ca}^{2+}$ -dependent activator (A) and inhibitor (I) enzymes.

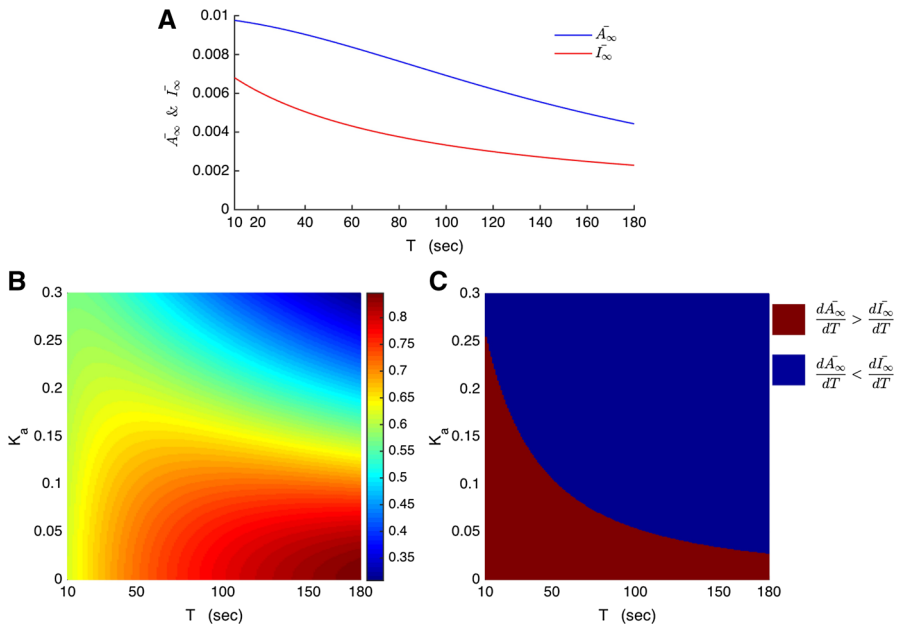


**Fig. 6** Relative sensitivity of the transcription factor to the activator and inhibitor enzymes determines the frequency response regime. **a** Representative  $\bar{A}_\infty$  (blue) and  $\bar{I}_\infty$  (red) curves. Relative positions of these curves determine the transcription factor activation level. **b** Approximate asymptotic fraction of the activated transcription factor ( $\overline{\text{TF}}_{ss}$ ) over a range of values of  $T$  and  $K_A$ . **c** The rates of changes of  $\bar{A}_\infty$  and  $\bar{I}_\infty$  with respect to  $T$  determines the frequency response. In the blue region,  $\bar{A}_\infty$  declines faster than  $\bar{I}_\infty$  as  $T$  is increased. In the brown region, this relation is reversed (Color figure online)

The time-dependent activation of enzymes is governed by Eqs. 1 and 2, and Eq. 3 describes the effect of the activated form of the enzymes ( $A_a$  and  $I_a$ ) on the fraction of activated transcription factor ( $\text{TF}_a$ ). For a periodic square-wave  $\text{Ca}^{2+}$  stimulus, the long-term mean values of  $A_a$  and  $I_a$  (denoted by  $\bar{A}_a$  and  $\bar{I}_a$ , respectively) are described by Eq. 12. Inserting these into Eqs. 4 and 5, respectively, yields  $\bar{A}_\infty$  and  $\bar{I}_\infty$  (Fig 6a). These long-term activator and inhibitor actions determine the approximate long-term or steady-state fraction of activated transcription factor:

$$\overline{\text{TF}}_{ss} = \frac{\bar{A}_\infty}{\bar{A}_\infty + \bar{I}_\infty}. \tag{19}$$

In the model, the sensitivity of the transcription factor to activator and inhibitor enzymes is determined by  $K_A$  and  $K_I$ , respectively (Table 1). Changes in these parameters shift the  $\bar{A}_\infty$  and  $\bar{I}_\infty$  curves left/right when plotted versus stimulus period as shown in Fig. 6a, and for each  $T$  value, the vertical distance between the curves is the primary determinant of the long-term transcription factor activation level (Eq. 19). That means the relative positions of these curves gives the fraction of activated transcription factor at each  $T$  value. Therefore, we explore frequency-dependent transcription factor dynamics by fixing  $\bar{I}_\infty$  and shifting  $\bar{A}_\infty$  horizontally by varying  $K_A$  (Fig. 6b). For

**Table 1** Parameter values

$p_A$	$0.1 \text{ s}^{-1}$	$C_m$	5300 fF
$n_A$	4	$\tau_n$	16 ms
$K_{cA}$	0.4	$f_{\text{cyt}}$	0.01
$d_A$	$0.004 \text{ s}^{-1}$	$f_{\text{er}}$	0.01
$p_I$	$0.1 \text{ s}^{-1}$	$V_{\text{cyt}}/V_{\text{er}}$	5
$n_I$	4	$\tau_a$	300 s
$K_{cI}$	0.4	$V_{\text{Ca}}$	25 mV
$d_I$	$0.004 \text{ s}^{-1}$	$V_K$	-75 mV
$\alpha_A$	$0.03 \text{ s}^{-1}$	$g_{\text{Ca}}$	1200 pS
$K_a$	0.8	$g_K$	3000 pS
$\beta_I$	$0.03 \text{ s}^{-1}$	$g_{K_{\text{ATP}}}$	142 pS
$K_i$	0.1	$g_{K_{\text{Ca}}}$	400 pS
$c_0$	$0.1 \text{ }\mu\text{M}$	$g_l$	170 pS
$p_M$	$0.001 \text{ s}^{-1}$	$K_\omega$	$0.3 \text{ }\mu\text{M}$
$K_m$	0.8	$\alpha$	$4.5 \times 10^{-6} \text{ ms}^{-1}$
$d_M$	$0.001 \text{ s}^{-1}$	$k_{\text{pmca}}$	$0.2 \text{ ms}^{-1}$
$p_g$	$0.02 \text{ pS s}^{-1}$	$p_{\text{leak}}$	$0.0005 \text{ ms}^{-1}$
$K_g$	0.8	$k_{\text{serca}}$	$0.4 \text{ ms}^{-1}$
$d_g$	$0.00265 \text{ s}^{-1}$		

small values of  $K_A$ , increasing frequency by moving from right to left reduces  $\overline{\text{TF}}_{ss}$  (Fig. 6b, bottom portion), while for large  $K_A$  values increasing frequency increases  $\overline{\text{TF}}_{ss}$  (Fig. 6b, top portion). For moderate  $K_A$  values, the frequency response of  $\overline{\text{TF}}_{ss}$  is bell shaped. Thus, for moderate  $K_A$  values there exists an optimum frequency for which  $\overline{\text{TF}}_{ss}$  is maximized (Fig. 6b, middle portion). To understand these relationships, we compare the rate of change of  $\bar{A}_\infty$  with respect to period  $T$  to that of  $\bar{I}_\infty$  as  $K_A$  is varied. Both  $\bar{A}_\infty$  and  $\bar{I}_\infty$  are decreasing functions of  $T$ , but in the brown region of Fig. 6c the rate of change of  $\bar{A}_\infty$  with respect to  $T$  is greater than the rate of change of  $\bar{I}_\infty$ . Therefore, in this region, as the frequency is increased (or as  $T$  is decreased),  $\bar{A}_\infty$  grows less than  $\bar{I}_\infty$  and inhibition dominates. Consequently, for small  $K_A$  values, increasing frequency reduces  $\overline{\text{TF}}_{ss}$ . In the blue region, this relation is reversed and increased frequency leads to a greater increase in  $\bar{A}_\infty$ . Therefore, for large  $K_A$  values, increasing frequency increases  $\overline{\text{TF}}_{ss}$ . For moderate  $K_A$  values, there is a transition from one region to the other as frequency is increased. Therefore, increasing frequency initially has a greater impact on  $\bar{A}_\infty$  than  $\bar{I}_\infty$  (blue region), which leads to a net increase in  $\overline{\text{TF}}_{ss}$ . Once in the brown region, further increasing frequency causes  $\overline{\text{TF}}_{ss}$  to decrease. In summary, depending on their sensitivities to the  $\text{Ca}^{2+}$  regulated enzymes, the transcription factor activity may increase or decrease with the frequency of the  $\text{Ca}^{2+}$  signal. If the sensitivity of the transcription factor to the inhibitor is greater than its sensitivity to the activator, then increased frequency increases transcription factor activation. When sensitivity of the transcription factor to the activator and the inhibitor are relatively similar, then the frequency response curve of the transcription factor is bell shaped and has an optimum range for stimulus frequency.

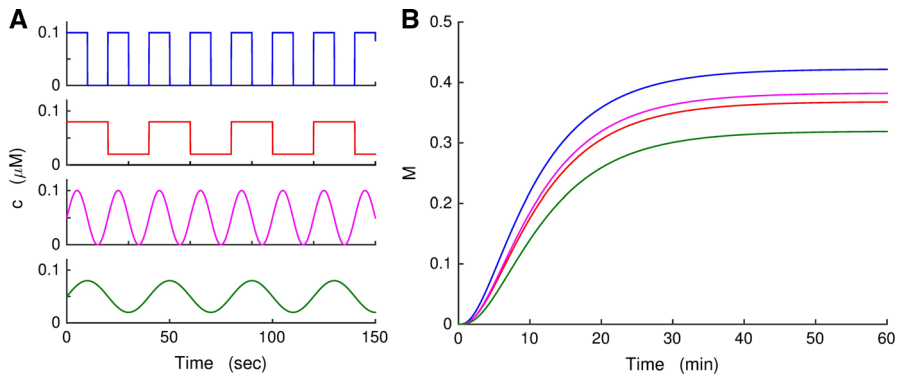


**Fig. 7** Different periodic  $\text{Ca}^{2+}$  signals produce different levels of gene expression, even though the average  $\text{Ca}^{2+}$  level is the same. **a** Two square-wave and two sinusoidal  $\text{Ca}^{2+}$  signals, each with the same average of  $0.05 \mu\text{M}$ . **b** The asymptotic mRNA level in response to the four  $\text{Ca}^{2+}$  stimuli (Color figure online)

The transcription factor is assumed to be an activator, so that its activated form,  $\text{TF}_a$ , increases the mRNA concentration. In the model, we describe the mRNA level with a dimensionless variable  $M$ , which changes in time according to:

$$\frac{dM}{dt} = p_M \frac{\text{TF}_a}{\text{TF}_a + K_M} - d_M M \quad (20)$$

where  $p_M$  is the maximal transcription rate,  $K_M$  is the  $\text{TF}_a$  for half-maximal transcription and  $d_M$  is the degradation rate. From the analysis above, it is clear that the level of activated transcription factor, and from Eq. 20 the level of mRNA, will be different with different patterns of square-wave input. This is shown in the red and blue traces of Fig. 7, where the stimulus frequencies and amplitudes are different, but the mean levels of  $\text{Ca}^{2+}$  are the same. In this case, the blue pattern evokes a larger response in the mRNA level (panel B). This is also true for the response to sinusoidal (violet and green) versus square-wave (blue and red) stimuli. Clearly, both the shape of the pulses and their frequency influence the mRNA level.

### 3.5 $\text{Ca}^{2+}$ Frequency-Dependent Upregulation of a Compensating Channel Can Rescue Bursting upon K(ATP) Knockout

We now ask whether, in a  $\beta$ -cell model adopted from (Bertram and Sherman 2004), knockout of the key K(ATP) ion channel can induce compensating upregulation of a different  $\text{K}^+$  ion channel to the correct level so that bursting electrical activity is rescued. Can the  $\text{Ca}^{2+}$ -dependent transcription described above act as a homeostatic mechanism to return the system to its original pattern of activity? An illustration of the model that shows the pathways regulating membrane potential is given in Fig. 8a. The model wild-type cell can produce bursting electrical activity by coupling a Hodgkin–Huxley-type membrane potential model with intracellular  $\text{Ca}^{2+}$  and nucleotide dynamics. It is equipped with voltage-gated  $\text{Ca}^{2+}$  and  $\text{K}^+$  currents ( $I_{\text{Ca}}$ ,  $I_{\text{K}}$ ), ATP- and  $\text{Ca}^{2+}$ -sensitive  $\text{K}^+$  currents ( $I_{\text{KATP}}$ ,  $I_{\text{KCa}}$ ), a leak current ( $I_l$ ) and an

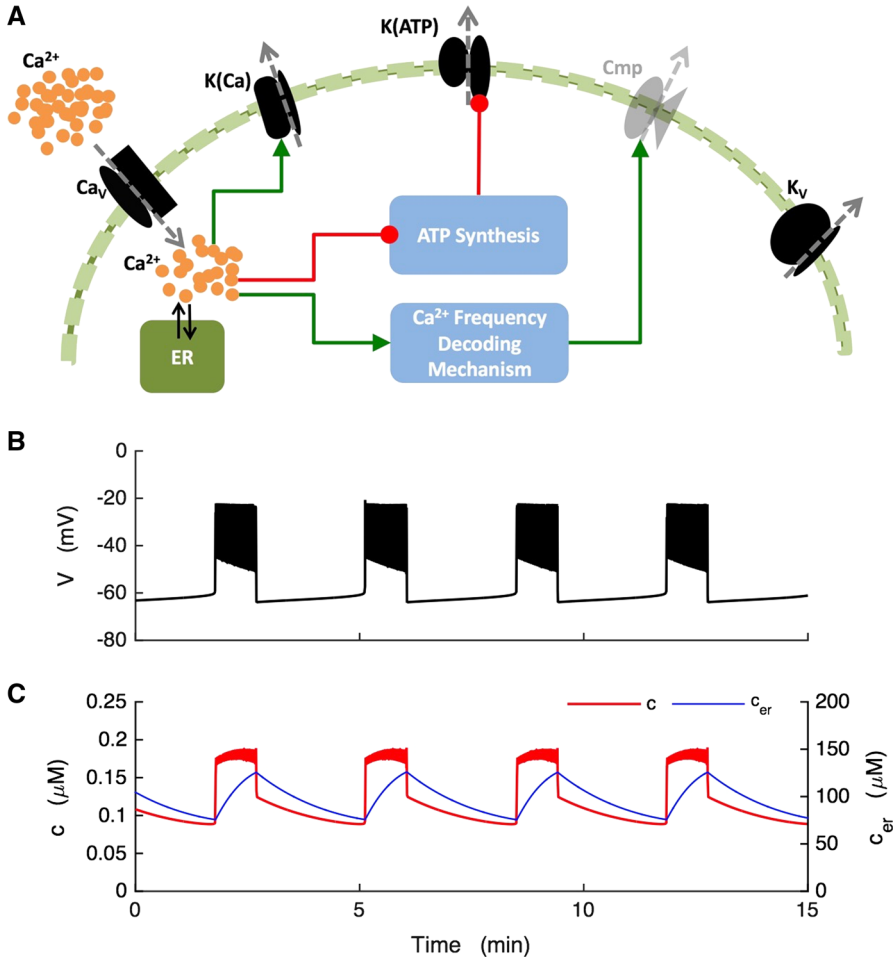


**Fig. 8** The model  $\beta$ -cell produces bursts of electrical activity accompanied by oscillations in the free cytosolic  $\text{Ca}^{2+}$  concentration ( $c$ ) and the free ER  $\text{Ca}^{2+}$  concentration ( $c_{\text{er}}$ ). **a** An illustration of the  $\beta$ -cell model. *Green arrows* represent stimulatory, and *red circles* represent inhibitory pathways. **b** The model cell produces bursts of electrical activity with a period of  $\sim 3$  min. **c** Bursts of electrical activity are accompanied by square-wave  $c$  oscillations (*red*) and slow sawtooth-shaped  $c_{\text{er}}$  oscillations (*blue*) (Color figure online)

inward-rectifying  $\text{K}^+$  current ( $I_{\text{cmp}}$ ). Inclusion of  $I_{\text{cmp}}$  is motivated by data discussed in Introduction on inward-rectifying Kir2.1 channel upregulation in mouse  $\beta$ -cells lacking K(ATP) channels. This current has a very small influence on the electrical activity of the wild-type cells, but is larger and gains importance during compensation. The differential equations for the electrical potential change across the plasma membrane,  $V$ , delayed-rectifying  $\text{K}^+$  current activation,  $n$ , the cytosolic ADP/ATP ratio,  $a$ , and the free cytosolic  $\text{Ca}^{2+}$  concentration,  $c$ , and free endoplasmic reticulum (ER)  $\text{Ca}^{2+}$  concentration,  $c_{\text{er}}$ , are as follows:

$$\frac{dV}{dt} = -(I_{Ca} + I_K + I_{K_{ATP}} + I_{K_{Ca}} + I_l + I_{cmp}) / C_m \quad (21)$$

$$\frac{dn}{dt} = (n_\infty(V) - n) / \tau_n \quad (22)$$

$$\frac{dc}{dt} = f_{cyt} (J_{mem} + J_{er}) \quad (23)$$

$$\frac{dc_{er}}{dt} = -f_{er} \frac{V_{cyt}}{V_{er}} J_{er} \quad (24)$$

$$\frac{da}{dt} = (a_\infty(c) - a) / \tau_a \quad (25)$$

where  $C_m$  is the constant membrane capacitance.  $n_\infty(V)$  and  $a_\infty(c)$  are the equilibrium functions for activation variables  $n$  and  $a$ , respectively,  $\tau_n$  and  $\tau_a$  are activation time constants,  $J_{mem}$  is the  $Ca^{2+}$  flux across the membrane and  $f_{cyt}$  is the ratio of unbound  $Ca^{2+}$  to the total  $Ca^{2+}$  concentration.  $J_{er}$  is the  $Ca^{2+}$  flux across the ER membrane, and  $f_{er}$  is the ratio of unbound  $Ca^{2+}$  to the total  $Ca^{2+}$  concentration in the ER.  $V_{cyt}$  and  $V_{er}$  are the volumes of cytosolic and ER compartments, respectively. The details of the equilibrium activation functions, ionic currents and fluxes are given in ‘‘Appendix 2.’’

When exposed to stimulatory glucose levels, pancreatic  $\beta$ -cells exhibit bursting electrical activity and  $Ca^{2+}$  oscillations. The model cell can produce bursting for moderate maximal conductance values of the ATP-sensitive  $K^+$  current (Fig. 8b). In the model, the fast activation of depolarizing  $Ca^{2+}$  current and slower activation of hyperpolarizing  $K^+$  current produces action potentials. Episodes of action potentials are separated by slow negative feedback provided by  $Ca^{2+}$  on the membrane potential and ATP production. The endoplasmic reticulum (ER) acts as a  $Ca^{2+}$  sink during active phases of spiking and as a  $Ca^{2+}$  source during silent phases. The impact that this buffering has on the cytosolic  $Ca^{2+}$  ultimately sets the period of bursting; during an active phase,  $c_{er}$  slowly rises as it uptakes  $Ca^{2+}$ , thereby removing some of the  $Ca^{2+}$  from the cytosol that would otherwise terminate a burst quickly through actions on  $Ca^{2+}$ -activated  $K^+$  channels. During a silent phase,  $c_{er}$  slowly declines as it releases  $Ca^{2+}$  into the cytosol, thereby delaying the decline of  $c$  that will ultimately allow spiking to restart by deactivation of the same  $K(Ca)$  channels (Fig. 8c). A detailed analysis of this bursting mechanism is given in the following section where we discuss the compensation dynamics.

We assume that the maximal conductances of all ionic currents are constant, with the exception of that of the compensating current ( $g_{cmp}$ ). We assume that the maximal conductance of this current is proportional to the compensating channel expression and dynamically regulated by  $Ca^{2+}$ -dependent gene transcription with the following equation:

$$\frac{dg_{cmp}}{dt} = p_g \frac{M}{M + K_g} - d_g \quad (26)$$

where  $M$  is the mRNA level, whose dynamics are governed by Eq. 20,  $p_g$  is the maximal rate of production,  $K_g$  is the mRNA level for half-maximal production and  $d_g$  represents the saturated degradation rate (Drengstig et al. 2008; He et al. 2013;

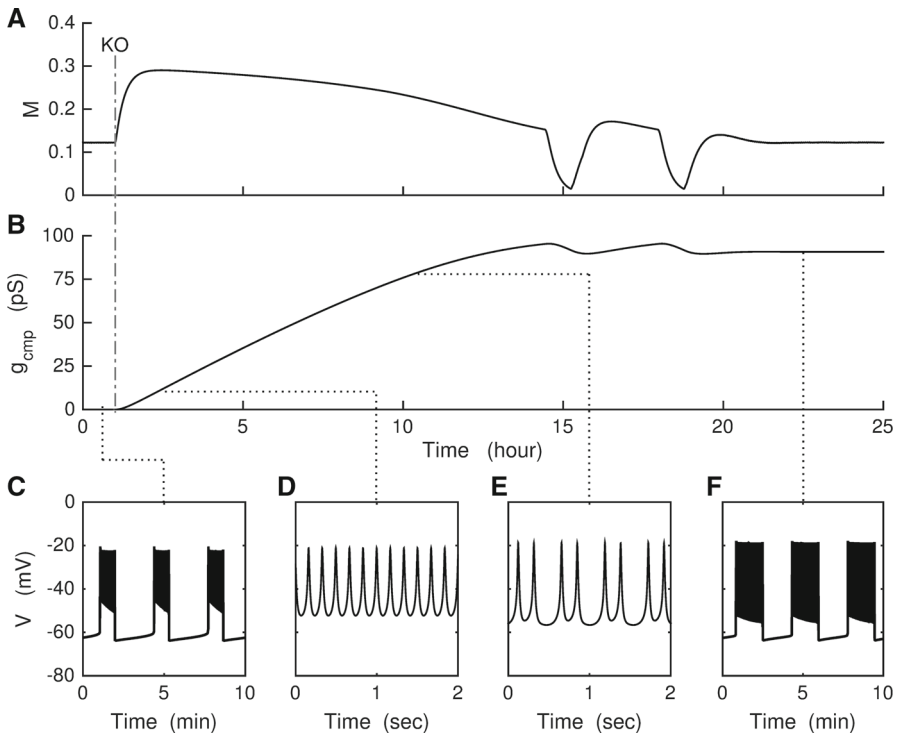


**Fig. 9** K(ATP) channel knockout changes the pattern of activity and leads to an increase in the expression of the compensating ion channel, eventually rescuing the bursting pattern. **a, b** Frequency decoding mechanism regulates  $M$ , which regulates  $g_{cmp}$ , according to the pattern of activity. Prior to the K(ATP) knockout (KO), the cell is in a homeostatic state with  $M$  and  $g_{cmp}$  at equilibrium levels. Once compensation is complete, a new homeostatic state is reached. Voltage traces show patterns of activity before KO (**c**), during compensation (**d, e**) and at the completion of compensation (**f**)

O’Leary et al. 2014). Dynamical regulation of  $g_{cmp}$  by  $Ca^{2+}$ -dependent transcription completes the feedback loop illustrated in Fig. 1.

We next examine the effect of K(ATP) channel knockout. Can the model cell successfully compensate for this and restore slow bursting? Prior to the knockout (KO) of K(ATP) channels (to the left of the dot-dashed line in Fig. 9), the cell is in a homeostatic state. The cell bursts with a period of about 3 min (Fig. 9c), and this pattern leads to a certain level of  $M$  (Fig. 9a, left of the KO). Parameter values are set so that at this homeostatic state  $g_{cmp}$  is low and constant (Fig. 9b, left of the KO). Since the burst pattern generated in this state is the behavior of the wild-type cell in the homeostatic state, we refer to it as ‘the target pattern of activity’. Following the knockout, the complete loss of hyperpolarizing K(ATP) current puts the cell into a continuously spiking depolarized state (Fig. 9d). This change in the pattern of activity alters the  $Ca^{2+}$  signal and consequently gene expression (Fig. 9a, right of the KO). Since the cytosolic  $Ca^{2+}$  level is now higher than before, both the mRNA level,  $M$ , of the compensating ion channel and the channel conductance,  $g_{cmp}$ , increase (Fig. 9b, right of the KO). Since the compensating current is a hyperpolarizing  $K^+$  current, increased

maximal conductance hyperpolarizes the cell membrane and slowly changes the pattern of activity (Fig. 9e). The hyperpolarization is accompanied by decreased  $\text{Ca}^{2+}$  concentration, which slows down production of  $M$ . At about hour 14 and again at about hour 18 following the knockout, there is a sharp decrease in the mRNA. This is due to the overexpression of the compensating current, which puts the cell into a transient silent state, where the  $\text{Ca}^{2+}$  level is low. As a result, both  $M$  and  $g_{\text{cmp}}$  decline. The latter decline causes electrical activity to re-emerge and the process continues as before. Within several more hours, a new homeostatic state is reached, and in this new state the cell is once again bursting with a period close to that of the target pattern of activity (Fig. 9f). There is a difference between burst periods and between the burst duty cycles, but this is to be expected since the properties of the compensating ion channel are not the same as those of the K(ATP) channel in the wild-type cell. In fact, electrophysiological recordings from wild-type and KO-mice islets also show noticeable differences in the bursting patterns (Düfer et al. 2004).

### 3.6 The Evolution of Dynamics in the Model $\beta$ -Cell During Compensation

To understand the way the dynamics of the model  $\beta$ -cell evolve throughout compensation, we performed a fast/slow analysis (Rinzel and Ermentrout 1998; Bertram et al. 1995). This method is widely used for analyzing the dynamics of systems that exhibit multi-timescale oscillations. The method separates the system of equations into two subsystems, a slow and a fast subsystem, with respect to the time scales on which variables change. The idea is that the slow variables remain relatively unchanged on the timescale of the fast variables. Therefore, initially, slow variables can be treated as the parameters of the fast subsystem and the dynamics of the fast subsystem can be explored as those parameters are changed. In the  $\beta$ -cell model that we use, the fast variables are voltage ( $V$ ), the activation variable for the voltage-gated  $\text{K}^+$  current ( $n$ ) and the cytosolic  $\text{Ca}^{2+}$  concentration ( $c$ ). The  $\text{Ca}^{2+}$  concentration in the ER ( $c_{\text{er}}$ ) and the cytosolic  $ADP/ATP$  ratio ( $a$ ) change more slowly. If we set  $a$  to its mean value over a burst period, the cell continues to burst with almost the same pattern. Therefore, we set  $a$  to its mean over a burst period, which reduces the number of slow variables to one and simplifies the analysis. The slow variable  $c_{\text{er}}$  acts on the fast subsystem through its effects on  $c$ , which in turn affects the membrane potential via the K(Ca) current.

The fast-subsystem bifurcation diagram of the model wild-type cell, using  $c_{\text{er}}$  as the bifurcation parameter, is shown in Fig. 10a. We refer to this as the “z-curve.” At low values of  $c_{\text{er}}$ , the fast subsystem produces continuous spiking, with the minimum and maximum value of  $V$  shown as blue curves in the bifurcation diagram. This spiking branch terminates at a homoclinic bifurcation (HC), but before this the branch loses stability at a period-doubling (PD) bifurcation. For larger values of  $c_{\text{er}}$ , there is a single low-voltage stable equilibrium. The branch of stable equilibria (solid black curve) loses stability at a saddle-node bifurcation (SN1), giving rise to a branch of saddle points (dashed black curve). The saddle points transition to unstable nodes at a second saddle-node bifurcation (SN2). Between SN1 and PD, there is a region of bistability between the spiking branch and the lower stationary branch, which is key to the bursting.

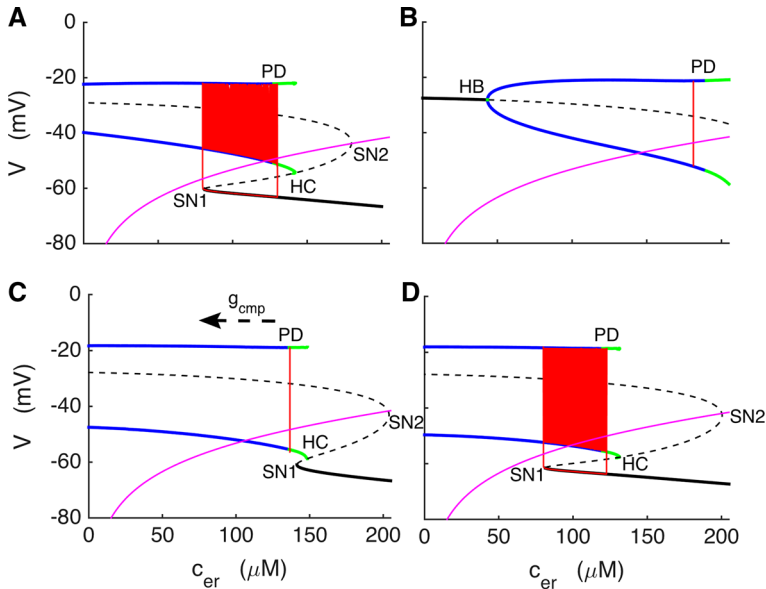


**Fig. 10** Fast/slow analysis of the model  $\beta$ -cell dynamics throughout the compensation process. The *black curve* represents stationary solutions of the fast subsystem, while the *blue curves* are the minimum and maximum voltage branches of periodic spiking solutions. The *green portions* of the periodic branch are regions in which the spiking branch is unstable. The *magenta curve* is the  $c_{er}$  nullcline, and the *red curve* is the projection of the asymptotic periodic orbit. **a** Before K(ATP) channel knockout. **b, c** At different points in the compensation process. **d** After completion of compensation. Panels **a–d** correspond to the time courses shown in Fig. 9, panels **c–f**, respectively (Color figure online)

To analyze the bursting shown in Fig. 9c, we treat the  $c_{er} - V$  plane as a phase plane, and add in the  $c_{er}$ -nullcline, obtained by setting  $\frac{dc_{er}}{dt} = 0$ . This is satisfied by  $J_{er} = 0$ , so from Eq. 59 of “Appendix 2”,

$$c_{er} = \frac{(k_{SERCA} + p_{leak}) c}{p_{leak}} \tag{27}$$

and on the slow timescale  $c$  is in quasi-equilibrium with  $V$  (so that  $J_{mem} = 0$ ) and using Eq. 58, the  $c_{er}$ -nullcline becomes:

$$c_{er} = -\frac{\alpha (k_{serca} + p_{leak}) I_{Ca}}{p_{leak} k_{pmca}} \tag{28}$$

where  $I_{Ca}$  is a function of  $V$  (Eq. 45). This curve is superimposed onto the z-curve in Fig. 10a (magenta curve). Finally, we complete the picture by adding the burst trajectory (red curve). During the silent phase, the trajectory follows the stable stationary branch of the z-curve, moving leftward toward the  $c_{er}$ -nullcline. When the saddle-node bifurcation SN1 is reached, the trajectory quickly transitions to the spiking attractor and slowly drifts rightward toward the  $c_{er}$ -nullcline, which is now to the right of the phase point. This is the active phase of the burst, and it is terminated soon after when

the spiking branch loses stability (green) at the period-doubling bifurcation. The trajectory follows the stable period-two branch until this branch itself loses stability at a second period-doubling bifurcation, and at this point the trajectory returns to the stable stationary branch, reentering the silent phase.

When the K(ATP) channel knockout is simulated ( $g_{K(ATP)} = 0$  pS), while the compensating channel conductance is still low ( $g_{cmp} = 5$  pS), the z-curve is shifted rightward due to the loss of hyperpolarizing current (Fig. 10b), now revealing the supercritical Hopf bifurcation (HB) from which the spiking branch emerges (the stable stationary branch is out of the viewing frame). The system moves to a new stable limit cycle consisting of continuous spiking (Fig. 10b, red curve), with time course shown in Fig. 9d. The spiking orbit is located at a value of  $c_{er}$  for which the average voltage of the spike is on the  $c_{er}$ -nullcline. Thus, without compensation, the knockout model cell would not burst, but would spike continuously.

Meanwhile, on a much slower timescale the compensation mechanism increases the expression of the compensating channel, shifting the z-curve leftward with the addition of hyperpolarizing current (Fig. 10c). The periodic orbit now comes to rest on a portion of the periodic branch where the continuous spiking solution is unstable, but the period-two solution is stable. This results in spike doublets, as shown in Fig. 9e. Eventually, when  $g_{cmp}$  rises to a sufficiently large value, compensation restores bursting (shown in Fig. 9f) with a dynamic mechanism essentially the same as in the wild-type cell (Fig. 10d).

### 3.7 The Model Predicts a Silencing Effect Following Prolonged Pharmacological Blockade of K(ATP) Channels

Experimental evidence suggests that pharmacological long-term blockade of the K(ATP) channels could lead to increased gene expression (Sjöholm 1995). Thus, upregulation of the compensating current may result from long-term pharmacological blockade of K(ATP) channels. Unlike the genetic knockout, the pharmacological blockade of the K(ATP) channels with an agent such as tolbutamide would be transient and reversible.

Figure 11 shows the effects of simulated blockade of K(ATP) channels. The model cell is initially bursting, but when K(ATP) channels are blocked (red dashed line) the cell immediately begins to spike continuously, leading to an elevated cytosolic  $Ca^{2+}$  level (Fig. 11b), which causes increased expression of the compensating channel and consequent increase in the channel conductance (Fig. 11a). The sharp rise in  $c$  after K(ATP) blockade is followed by a gradual decay, which is due to the slow rise in the compensating current that has a hyperpolarizing effect on the cell membrane. After removal of the K(ATP) channel blocker (vertical green dashed line), the cell remains silent for roughly an hour, which results in a sustained low value of  $c$ . This prolonged silent period is due to the combination of the restored K(ATP) current and the compensating  $K^+$  current,  $I_{cmp}$ . With the low value of  $c$ , however,  $g_{cmp}$  declines and after some time  $I_{cmp}$  is small enough that bursting resumes, although initially with a lower frequency. The longer the application of K(ATP) channel blocker, the longer

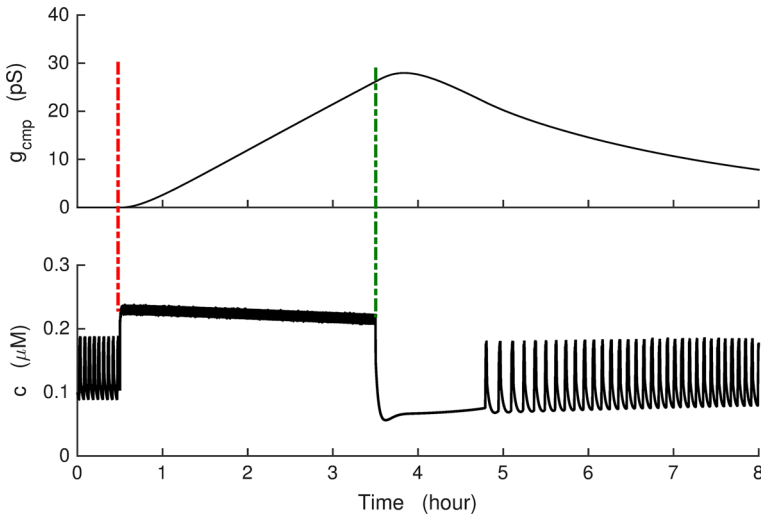


**Fig. 11** K(ATP) current is transiently turned off at the vertical red dashed line and turned back on at the vertical green dashed line. **a** The compensating current conductance. **b** The  $c$  time course, showing a transient silencing after K(ATP) current is added back (Color figure online)

the silent phase after its removal. The prolonged hyperpolarized phase that follows K(ATP) channel restoration is a testable model prediction.

## 4 Discussion

In this report, we introduced an activity-dependent homeostatic compensation mechanism to explain the rescue of bursting electrical activity observed in K(ATP) channel-deficient pancreatic mouse  $\beta$ -cells (Fig. 9). The mechanism for compensation is based on  $\text{Ca}^{2+}$  activation of two opposing enzymes that control the level of gene expression of the compensating channel, which is altered when the K(ATP) channels are removed. It is well established that long-term changes in the activity of an excitable cell can regulate the expression of ion channels (LeMasson et al. 1993; Rosati and McKinnon 2004; O'Leary et al. 2014). This may result from the increased intracellular  $\text{Ca}^{2+}$  concentration, which is a well-documented regulator of gene expression (Barish 1998; West et al. 2001). One safety aspect of the feedback mechanism is that it prevents the cytosolic  $\text{Ca}^{2+}$  concentration from remaining persistently elevated, which leads to excitotoxicity and ultimately cell death (Efanova et al. 1998; Iwakura et al. 2000; Maedler et al. 2005; Pinton et al. 2008). Our model responds to the K(ATP) channel knockout by regulating the expression of a compensating inward-rectifier  $\text{K}^+$  channel. Such channels, Kir2.1, have been shown to be upregulated in K(ATP) knockout cells (manuscript in preparation), and the upregulated channels are functional, providing inward-rectifying current (manuscript submitted). In the model, the key elements are two opposing  $\text{Ca}^{2+}$ -dependent enzymes, which decode the frequency of the  $\text{Ca}^{2+}$  oscillations and regulate the activity of a target transcription factor. These enzymes could be either kinases or phosphatases, both of which have  $\text{Ca}^{2+}$ -dependent isoforms

(Rosen et al. 1995; Swulius and Waxham 2013; Li et al. 2011). Studies have shown that some  $\text{Ca}^{2+}$ -frequency-sensitive transcription factors are activated when phosphorylated (Segil et al. 1991; Oeckinghaus and Ghosh 2009) where others are activated when dephosphorylated (Rao et al. 1997).

It was previously shown that  $\text{Ca}^{2+}$  is more effective at regulating gene expression when delivered in an oscillatory fashion (Dolmetsch et al. 1998; Tsien et al. 1998). This amplifying effect of  $\text{Ca}^{2+}$  oscillations was subsequently studied with mathematical models (Dupont et al. 2003; Schuster et al. 2005; Salazar et al. 2008). These studies show that the efficiency of the oscillatory signals arises primarily from the nonlinear dependence of the components of the pathway on the upstream events, which may result from cooperative  $\text{Ca}^{2+}$  binding, zero-order ultra-sensitivity, homo-dimerization or trimerization and cooperative activation through multiple pathways (Zhang et al. 2013). These prior modeling studies either focused on the transcription factors which are regulated by a single  $\text{Ca}^{2+}$ -dependent enzyme (Salazar et al. 2008) or focus on the activation of the enzymes themselves (Dupont et al. 2003). However, activity of several transcription factors is modulated by multiple pathways that involve  $\text{Ca}^{2+}$ -dependent components (Berridge et al. 2003). We showed that regulation of a transcription factor by two opposing  $\text{Ca}^{2+}$ -dependent enzymes yields qualitatively different frequency response regimes (Fig. 6). Depending on the relative affinities of the transcription factor to the activator and inhibitor enzymes, transcription factor activation may increase with the frequency of the stimulus or decrease. If the transcription factor's sensitivity to the activator and inhibitor enzymes are comparable, then there is bell-shaped response function with an optimum frequency for which the activation of the transcription factor is maximized, as has been observed experimentally (Tsien et al. 1998; Zhu et al. 2008).

The compensation mechanism that we employed differs fundamentally from the mechanism described in (O'Leary et al. 2014). In that study, gene expression evolved to a point such that the time-averaged  $\text{Ca}^{2+}$  concentration matched a target level. In the mechanism that we employed, there is no explicit target, and the  $\text{Ca}^{2+}$  pattern, not its time average, sets the expression level of the compensating gene (Fig. 7). Parameter values were set so that the interaction of the activator and inhibitor enzymes push the system to a point such that the  $\text{Ca}^{2+}$  concentration oscillates and the pattern is similar to that of wild-type cells. We speculate that in the actual cells this choice of affinity values would be set through natural selection, given the importance of pulsatile insulin secretion in glucose homeostasis (Matthews et al. 1983b; Paolisso et al. 1991; Hellman 2009; Matveyenko et al. 2012).

While we have considered compensation through a single gene, the reality is much more complicated. Studies have shown that the expression levels are altered for tens or hundreds of genes in response to genetic knockout of a single gene (Liu et al. 2007; Eraly 2014; Wang et al. 2015). The difficulty comes in determining which of these changes are the most important for the behavior of the cell. In the case of K(ATP) channel knockout in pancreatic  $\beta$ -cells, we know that Kir2.1 channels are upregulated (manuscript in preparation), but there are likely many other changes in protein levels, some of which could be ion channels. Mathematical modeling can be useful here, in determining which channels can potentially compensate for the K(ATP) channel in the preservation of electrical bursting activity. We recently showed that Kir2.1 has the right properties to do this (manuscript submitted), but we gave no explanation for how the

cell would know how much Kir2.1 conductance was needed to rescue bursting. How would the appropriate level of expression of this compensating channel be determined? That question motivated the current study, in which we showed that the appropriate level of compensation can occur quite naturally provided that the transcription factor is activated by  $\text{Ca}^{2+}$ -dependent enzymes whose levels of activation are different for  $\text{Ca}^{2+}$  signals of different frequencies. That is,  $\text{Ca}^{2+}$ -frequency regulated enzymes. This process would of course be much more complex if the expression levels of multiple ion channel proteins or modulating enzymes are affected by the compensation process, but the same underlying principle should apply. Indeed, having several degrees of freedom should make it easier to achieve a target pattern that is similar to that of the wild-type cell.

It has been shown that long-term blockade of K(ATP) channels by pharmacological agents in insulin-secreting cell lines results in increased DNA synthesis (Sjöholm 1995). The same study showed that blocking  $\text{Ca}^{2+}$  influx, while K(ATP) channels are blocked, suppressed the DNA synthesis. This is direct evidence for  $\text{Ca}^{2+}$ -dependent compensatory gene expression in response to the removal of K(ATP) current. We simulated transient K(ATP) blockage and found that the cell is silenced for an extended period of time after the channel blocker is removed (Fig. 11). The duration of the silent phase increases with the length of time that K(ATP) channels remain blocked. While K(ATP) channel blockers such as tolbutamide have been used in many studies [for example, (Larsson et al. 1996; Ren et al. 2013)], the exposure time is typically in the seconds to minutes range. A recent study applied tolbutamide to islets overnight, but the behavior of the islets immediately after removal of the channel blocker was not examined (Glynn et al. 2016). Thus, our finding of cell silencing after hours-long blockade of K(ATP) channels is a testable, but to our knowledge untested, prediction.

**Acknowledgements** This work was partially supported by a Grant from the National Science Foundation (DMS-1612193) to R.B.

## Appendix 1

The linear differential equation (Eq. 7) that governs the rate of change of the fraction of an activated enzyme has the following form:

$$\frac{dE_a}{dt} = p_E \frac{c^{n_E}}{c^{n_E} + K_E^{n_E}} (1 - E_a) - d_E E_a. \quad (29)$$

This can be solved in response to the following square-wave  $\text{Ca}^{2+}$  stimulus:

$$c(t) = \begin{cases} c_0 = 0.1, & \text{mod}(t, T) \leq D \\ 0, & \text{mod}(t, T) > D \end{cases} \quad (30)$$

Derivation of the solution is similar to what was done in prior studies (Schuster et al. 2005; Salazar et al. 2008). The solution during the  $i$ th oscillation cycle is:

$$E_{a,i}(\theta) = \begin{cases} E_{ss} + \xi_i e^{-(p_E^* + d_E)\theta}, & 0 \leq \theta < D \\ \psi_i e^{-d_E\theta}, & D \leq \theta \leq T \end{cases} \quad (31)$$

where  $E_{a,i}$  is the solution of Eq. 29 for the  $i$ th stimulus cycle with the internal time  $\theta \in [0, T]$  and  $E_{ss}$  and  $p_E^*$  are given by:

$$p_E^* = pE \frac{c_0^{nE}}{c_0^{nE} + K_E^{nE}}, \quad (32)$$

$$E_{ss} = \frac{1}{1 + \frac{d_E}{p_E^*}}. \quad (33)$$

For consecutive oscillation cycles  $i - 1$  and  $i$ ,

$$E_{a,i-1}(T) = E_{a,i}(0) \quad (34)$$

and  $E_{a,i}$  is continuous at  $D$ . Therefore, these relations yield the following difference equations for coefficients  $\xi_i$  and  $\psi_i$ :

$$\xi_{i+1} = E_{ss} \left( e^{-d_E(T-D)} - 1 \right) + e^{-(p_E^*D+d_ET)} \xi_i \quad (35)$$

$$\psi_i = e^{-p_E^*D} \xi_i + E_{ss} e^{-d_ED}. \quad (36)$$

Assuming that the enzyme is completely in its inactive form at the beginning,  $E_{a,0}(0) = 0$ , we get  $\xi_0 = -E_{ss}$ . The difference equation in Eq. 35 has the form,

$$x_{i+1} = ax_i + b \quad (37)$$

and with initial condition  $x_0$ :

$$\begin{aligned} x_i &= ax_{i-1} + b \\ &= a(ax_{i-2} + b) + b \\ &= a^2x_{i-2} + ab + b \\ &= a^2(ax_{i-3} + b) + ab + b \\ &= a^3x_{i-3} + a^2b + ab + b \\ &\dots \\ x_i &= a^i x_0 + b \underbrace{\left( a^{i-1} + \dots + a^2 + a + 1 \right)}_{\frac{(a^i-1)}{a-1}} \end{aligned}$$

Hence,

$$x_i = a^i x_0 + \frac{b(a^i - 1)}{a - 1}. \quad (38)$$

Therefore, the solution to Eq. 35 is:

$$\xi_i = -e^{-(p_E^*D+d_E T)i} E_{ss} + \frac{E_{ss} (e^{-d_E(T-D)} - 1) (e^{-(p_E^*D+d_E T)i} - 1)}{e^{-(p_E^*D+d_E T)} - 1} \tag{39}$$

For  $i \rightarrow \infty$ ,

$$\xi_i \rightarrow \xi_\infty = -E_{ss} \frac{e^{-d_E(T-D)} - 1}{e^{-(p_E^*D+d_E T)} - 1} \tag{40}$$

and consequently,

$$\psi_i \rightarrow \psi_\infty = E_{ss} \frac{e^{d_E D} - e^{-p_E^* D}}{1 - e^{-(p_E^*D+d_E T)}}. \tag{41}$$

Thus, over many stimulus cycles the solution to Eq. 31 approaches:

$$E_{a,\infty}(\theta) = \begin{cases} E_{ss} + \xi_\infty e^{-(p_E^*+d_E)\theta}, & 0 \leq \theta < D^- \\ \psi_\infty e^{-d_E\theta}, & D^+ \leq \theta \leq T \end{cases}. \tag{42}$$

The mean fraction of activated enzyme concentration during this stimulus cycle is then given by:

$$\bar{E}_a = \frac{1}{T} \int_0^T E_{a,\infty}(\theta) d\theta, \tag{43}$$

or upon integration:

$$\bar{E}_a = E_{ss} \left( \frac{D}{T} + \frac{1}{d_E T} E_{ss} \frac{(1 - e^{-D(d_E+p_E^*)})(1 - e^{-d_E(T-D)})}{1 - e^{-(p_E^*D+d_E T)}} \right). \tag{44}$$

### Appendix 2

The  $\beta$ -cell model is from (Bertram and Sherman 2004) with the following ionic currents:

$$I_{Ca} = g_{Ca} m_\infty (V - V_{Ca}), \tag{45}$$

$$I_K = g_K n (V - V_K), \tag{46}$$

$$I_{K_{ATP}} = g_{K_{ATP}} a (V - V_K), \tag{47}$$

$$I_{K_{Ca}} = g_{K_{Ca}} \omega (V - V_K), \tag{48}$$

$$I_l = g_l (V - V_l), \tag{49}$$

$$I_{cmp} = g_{cmp} k_\infty (V - V_K). \tag{50}$$

For each ionic current  $I_i$ ,  $g_i$  is the maximal conductance,  $V_i$  is the reversal potential and  $(V - V_i)$  is the driving force. The rates of changes of the delayed rectifier  $K^+$  current activation,  $n$ , and the  $K(\text{ATP})$  current activation,  $a$ , are:

$$\frac{dn}{dt} = (n_\infty(V) - n) / \tau_n, \quad (51)$$

$$\frac{da}{dt} = (a_\infty(c) - a) / \tau_a, \quad (52)$$

where  $\tau_n$  and  $\tau_a$  are the time constants. Steady-state activation functions,  $m_\infty$ ,  $n_\infty$ ,  $a_\infty$  and  $k_\infty$ , are:

$$m_\infty(V) = \frac{1}{1 + e^{(-20-V)/12}}, \quad (53)$$

$$n_\infty(V) = \frac{1}{1 + e^{(-16-V)/5}}, \quad (54)$$

$$k_\infty(V) = \frac{1}{1 + e^{(-49-V)/15}}, \quad (55)$$

$$a_\infty(c) = \frac{1}{1 + e^{(0.14-c)/0.1}}, \quad (56)$$

where  $m_\infty$ ,  $n_\infty$ ,  $a_\infty$  and  $k_\infty$  are sigmoidal functions of  $V$  and  $c$ .  $\omega$  is the  $\text{Ca}^{2+}$ -dependent activation variable of  $I_{K_{Ca}}$  and given with the following Hill equation:

$$\omega = \frac{c^5}{c^5 + K_\omega^5}, \quad (57)$$

where  $K_\omega$  is the dissociation constant.  $\text{Ca}^{2+}$  fluxes across the plasma and endoplasmic reticulum (ER) membranes are:

$$J_{\text{mem}} = -(\alpha I_{Ca} + k_{\text{pmca}}c), \quad (58)$$

$$J_{\text{er}} = p_{\text{leak}}(c_{\text{er}} - c) - k_{\text{serca}}c, \quad (59)$$

where parameter  $\alpha$  converts ionic current to flux and provides  $\text{Ca}^{2+}$  influx through voltage-gated  $\text{Ca}^{2+}$  channels and  $k_{\text{pmca}}$  is the plasma membrane  $\text{Ca}^{2+}$ -ATPase pumping rate and mediates  $\text{Ca}^{2+}$  efflux from the cytosol.  $\text{Ca}^{2+}$  leaks from the ER with a rate proportional to  $p_{\text{leak}}$ .  $k_{\text{serca}}$  is the  $\text{Ca}^{2+}$  pumping rate into the ER by SERCA pumps.

## References

- Barish ME (1998) Intracellular calcium regulation of channel and receptor expression in the plasmalemma: Potential sites of sensitivity along the pathways linking transcription, translation, and insertion. *J Neurobiol* 37:146–157. doi:[10.1002/\(SICI\)1097-4695\(199810\)37:1<146::AID-NEU11>3.0.CO;2-C](https://doi.org/10.1002/(SICI)1097-4695(199810)37:1<146::AID-NEU11>3.0.CO;2-C)
- Berridge MJ, Bootman MD, Roderick HL (2003) Calcium signalling: dynamics, homeostasis and remodeling. *Nat Rev Mol Cell Biol* 4:517–529. doi:[10.1038/nrm1155](https://doi.org/10.1038/nrm1155)

- Bertram R, Butte MJ, Kiemel T, Sherman A (1995) Topological and phenomenological classification of bursting oscillations. *Bull Math Biol* 57:413–439. doi:[10.1007/BF02460633](https://doi.org/10.1007/BF02460633)
- Bertram R, Sherman A (2004) A calcium-based phantom bursting model for pancreatic islets. *Bull Math Biol* 66:1313–1344. doi:[10.1016/j.bulm.2003.12.005](https://doi.org/10.1016/j.bulm.2003.12.005)
- Bertram R, Sherman A, Satin LS (2010) Electrical bursting, calcium oscillations, and synchronization of pancreatic islets. *Adv Exp Med Biol* 654:261–279. doi:[10.1007/978-90-481-3271-3\\_12](https://doi.org/10.1007/978-90-481-3271-3_12)
- Bradshaw JM, Kubota Y, Meyer T, Schulman H (2003) An ultrasensitive  $\text{Ca}^{2+}$ /calmodulin-dependent protein kinase II-protein phosphatase 1 switch facilitates specificity in postsynaptic calcium signaling. *Proc Natl Acad Sci USA* 100:10512–10517. doi:[10.1073/pnas.1932759100](https://doi.org/10.1073/pnas.1932759100)
- Collins TJ, Lipp P, Berridge MJ, Bootman MD (2001) Mitochondrial  $\text{Ca}^{2+}$  uptake depends on the spatial and temporal profile of cytosolic  $\text{Ca}^{2+}$  signals. *J Biol Chem* 276:26411–26420. doi:[10.1074/jbc.M101101200](https://doi.org/10.1074/jbc.M101101200)
- Davis GW (2006) Homeostatic control of neural activity: from phenomenology to molecular design. *Annu Rev Neurosci* 29:307–323. doi:[10.1146/annurev.neuro.28.061604.135751](https://doi.org/10.1146/annurev.neuro.28.061604.135751)
- De Koninck P, Schulman H (1998) Sensitivity of CaM kinase II to the frequency of  $\text{Ca}^{2+}$  oscillations. *Science* 279:227–230. doi:[10.1126/science.279.5348.227](https://doi.org/10.1126/science.279.5348.227)
- Dolmetsch RE, Xu K, Lewis RS (1998) Calcium oscillations increase the efficiency and specificity of gene expression. *Nature* 392:933–936. doi:[10.1038/31960](https://doi.org/10.1038/31960)
- Drengstig T, Ueda HR, Ruoff P (2008) Predicting perfect adaptation motifs in reaction kinetic networks. *J Phys Chem B* 112:16752–16758. doi:[10.1021/jp806818c](https://doi.org/10.1021/jp806818c)
- Düfer M, Haspel D, Krippeit-Drews P, Aguilar-Bryan L, Bryan J, Drews G (2004) Oscillations of membrane potential and cytosolic  $\text{Ca}^{2+}$  concentration in  $\text{SUR1}^{-/-}$  beta cells. *Diabetologia* 47:488–498. doi:[10.1007/s00125-004-1348-0](https://doi.org/10.1007/s00125-004-1348-0)
- Dupont G, Goldbeter A (1998) CaM kinase II as frequency decoder of  $\text{Ca}^{2+}$  oscillations. *BioEssays* 20:607–610. doi:[10.1002/\(SICI\)1521-1878\(199808\)20:8<607::AID-BIES2>3.0.CO;2-F](https://doi.org/10.1002/(SICI)1521-1878(199808)20:8<607::AID-BIES2>3.0.CO;2-F)
- Dupont G, Houart G, De Koninck P (2003) Sensitivity of CaM kinase II to the frequency of  $\text{Ca}^{2+}$  oscillations: a simple model. *Cell Calcium* 34:485–497. doi:[10.1016/j.biosystems.2005.02.004](https://doi.org/10.1016/j.biosystems.2005.02.004)
- Efanova IB, Zaitsev SV, Zhivotovsky B, Köhler M, Efenđić S, Orrenius S, Berggren P-O (1998) Glucose and tolbutamide induce apoptosis in pancreatic  $\beta$ -cells: a process dependent on intracellular  $\text{Ca}^{2+}$  concentration. *J Biol Chem* 273:33501–33507. doi:[10.1074/jbc.273.50.33501](https://doi.org/10.1074/jbc.273.50.33501)
- Eraly SA (2014) Striking differences between knockout and wild-type mice in global gene expression variability. *PLoS One*. doi:[10.1371/journal.pone.0097734](https://doi.org/10.1371/journal.pone.0097734)
- Falcke M, Malchow D (2003) Understanding calcium dynamics: experiments and theory. Springer, Berlin
- Frieden C (1970) Kinetic aspects of regulation of metabolic processes. The hysteretic enzyme concept. *J Biol Chem* 245:5788–5799. doi:[10.1146/annurev.bi.48.070179.002351](https://doi.org/10.1146/annurev.bi.48.070179.002351)
- Frieden C (1979) Slow transitions and hysteretic behavior in enzymes. *Annu Rev Biochem* 48:471–489. doi:[10.1146/annurev.bi.48.070179.002351](https://doi.org/10.1146/annurev.bi.48.070179.002351)
- Glynn E, Thompson B, Vadrevu S, Lu S, Kennedy RT, Ha J, Sherman A, Satin LS (2016) Chronic glucose exposure systematically shifts the oscillatory threshold of mouse islets: experimental evidence for an early intrinsic mechanism of compensation for hyperglycemia. *Endocrinology* 157:611–623. doi:[10.1210/en.2015-1563](https://doi.org/10.1210/en.2015-1563)
- Hajnóczky G, Robb-Gaspers LD, Seitz MB, Thomas AP (1995) Decoding of cytosolic calcium oscillations in the mitochondria. *Cell* 82:415–424. doi:[10.1016/0092-8674\(95\)90430-1](https://doi.org/10.1016/0092-8674(95)90430-1)
- He F, Fromion V, Westerhoff HV (2013) (Im)Perfect robustness and adaptation of metabolic networks subject to metabolic and gene-expression regulation: marrying control engineering with metabolic control analysis. *BMC Syst Biol* 7:131. doi:[10.1186/1752-0509-7-131](https://doi.org/10.1186/1752-0509-7-131)
- Hedekov CJ (1980) Mechanism of glucose-induced insulin secretion. *Physiol Rev* 60(2):442–509. doi:[10.1146/annurev-physiol-030212-183754](https://doi.org/10.1146/annurev-physiol-030212-183754)
- Hellman B (2009) Pulsatility of insulin release—a clinically important phenomenon. *Ups J Med Sci* 114:193–205. doi:[10.3109/03009730903366075](https://doi.org/10.3109/03009730903366075)
- Iwakura T, Fujimoto S, Kagimoto S, Inada A, Kubota A, Someya Y, Ihara Y, Yamada Y, Seino Y (2000) Sustained enhancement of  $\text{Ca}^{2+}$  influx by glibenclamide induces apoptosis in RINm5F cells. *Biochem Biophys Res Commun* 271:422–428. doi:[10.1006/bbrc.2000.2616](https://doi.org/10.1006/bbrc.2000.2616)
- Kane C, Shepherd RM, Squires PE, Johnson PR, James RF, Milla PJ, Aynsley-Green A, Lindley KJ, Dunne MJ (1996) Loss of functional  $\text{K}_{\text{ATP}}$  channels in pancreatic  $\beta$ -cells causes persistent hyperinsulinemic hypoglycemia of infancy. *Nat Med* 2:1344–1347. doi:[10.1038/nm1296-1344](https://doi.org/10.1038/nm1296-1344)

- Larsson O, Kindmark H, Brandstrom R, Fredholm B, Berggren PO (1996) Oscillations in  $K_{ATP}$  channel activity promote oscillations in cytoplasmic free  $Ca^{2+}$  concentration in the pancreatic  $\beta$  cell. *Proc Natl Acad Sci USA* 93:5161–5165. doi:[10.1073/pnas.93.10.5161](https://doi.org/10.1073/pnas.93.10.5161)
- LeMasson G, Marder E, Abbott LF (1993) Activity-dependent regulation of conductances in model neurons. *Science* 259:1915–1917. doi:[10.1126/science.8456317](https://doi.org/10.1126/science.8456317)
- Li H, Rao A, Hogan PG (2011) Interaction of calcineurin with substrates and targeting proteins. *Trends Cell Biol* 21:91–103. doi:[10.1016/j.tcb.2010.09.011](https://doi.org/10.1016/j.tcb.2010.09.011)
- Li L, Stefan MI, Le Novère N (2012) Calcium input frequency, duration and amplitude differentially modulate the relative activation of calcineurin and CaMKII. *PLoS One*. doi:[10.1371/journal.pone.0043810](https://doi.org/10.1371/journal.pone.0043810)
- Liu DYT, Liu CH, Lai MT, Lin H-K, Hseu T-H (2007) Global gene expression profiling of wild type and lysC knockout *Escherichia coli* W3110. *FEMS Microbiol Lett* 276:202–206. doi:[10.1111/j.1574-6968.2007.00932.x](https://doi.org/10.1111/j.1574-6968.2007.00932.x)
- Liu Z, Golowasch J, Marder E, Abbott LF (1998) A model neuron with activity-dependent conductances regulated by multiple calcium sensors. *J Neurosci* 18:2309–2320
- Maedler K, Carr RD, Bosco D, Zuellig RA, Berney T, Donath MY (2005) Sulfonylurea induced  $\beta$ -cell apoptosis in cultured human islets. *J Clin Endocrinol Metab* 90:501–506. doi:[10.1210/jc.2004-0699](https://doi.org/10.1210/jc.2004-0699)
- Matthews DR, Lang DA, Burnett MA, Turner RC (1983a) Control of pulsatile insulin secretion in man. *Diabetologia* 24:231–237. doi:[10.1007/BF00282705](https://doi.org/10.1007/BF00282705)
- Matthews DR, Naylor BA, Jones RG (1983b) Pulsatile insulin has greater hypoglycemic effect than continuous delivery. *Diabetes* 37:617–621. doi:[10.2337/diabetes.32.7.617](https://doi.org/10.2337/diabetes.32.7.617)
- Matveyenko AV, Liuwantara D, Gurlo T, Kirakossian D, Dalla Man C, Cobelli C, White MF, Copps KD, Volpi E, Fujita S, Butler PC (2012) Pulsatile portal vein insulin delivery enhances hepatic insulin action and signaling. *Diabetes* 61:2269–2279. doi:[10.2337/db11-1462](https://doi.org/10.2337/db11-1462)
- Matveyenko AV, Veldhuis JD, Butler PC (2008) Measurement of pulsatile insulin secretion in the rat: direct sampling from the hepatic portal vein. *Am J Physiol* 295:E569–E574. doi:[10.1152/ajpendo.90335.2008](https://doi.org/10.1152/ajpendo.90335.2008)
- McKenna JP, Ha J, Merrins MJ, Satin LS, Sherman A, Bertram R (2016)  $Ca^{2+}$  effects on ATP production and consumption have regulatory roles on oscillatory islet activity. *Biophys J* 110:733–742. doi:[10.1016/j.bpj.2015.11.3526](https://doi.org/10.1016/j.bpj.2015.11.3526)
- Merrins MJ, Poudel C, McKenna JP, Ha J, Sherman A, Bertram R, Satin LS (2016) Phase analysis of metabolic oscillations and membrane potential in pancreatic islet  $\beta$ -cells. *Biophys J* 110:691–699. doi:[10.1016/j.bpj.2015.12.029](https://doi.org/10.1016/j.bpj.2015.12.029)
- Nenquin M, Szollosi A, Aguilar-Bryan L, Bryan J, Henquin JC (2004) Both triggering and amplifying pathways contribute to fuel-induced insulin secretion in the absence of sulfonylurea receptor-1 in pancreatic  $\beta$ -cells. *J Biol Chem* 279:32316–32324. doi:[10.1074/jbc.M402076200](https://doi.org/10.1074/jbc.M402076200)
- Nichols CG (2006)  $K_{ATP}$  channels as molecular sensors of cellular metabolism. *Nature* 440:470–476. doi:[10.1038/nature04711](https://doi.org/10.1038/nature04711)
- Nunemaker CS, Zhang M, Wasserman DH, McGuinness OP, Powers AC, Bertram R, Sherman A, Satin LS (2005) Individual mice can be distinguished by the period of their islet calcium oscillations: is there an intrinsic islet period that is imprinted in vivo? *Diabetes* 54:3517–3522. doi:[10.2337/diabetes.54.12.3517](https://doi.org/10.2337/diabetes.54.12.3517)
- O’Leary T, Williams AH, Franci A, Marder E (2014) Cell types, network homeostasis, and pathological compensation from a biologically plausible ion channel expression model. *Neuron* 82:809–821. doi:[10.1016/j.neuron.2014.04.002](https://doi.org/10.1016/j.neuron.2014.04.002)
- O’Rahilly S, Turner RC, Matthews DR (1988) Impaired pulsatile secretion of insulin in relatives of patients with non-insulin-dependent diabetes. *N Engl J Med* 318:1225–1230. doi:[10.1056/NEJM198805123181902](https://doi.org/10.1056/NEJM198805123181902)
- Oeckinghaus A, Ghosh S (2009) The NF- $\kappa$ B family of transcription factors and its regulation. *Cold Spring Harb Perspect Biol* 1:a000034. doi:[10.1101/cshperspect.a000034](https://doi.org/10.1101/cshperspect.a000034)
- Olypher AV, Prinz AA (2010) Geometry and dynamics of activity-dependent homeostatic regulation in neurons. *J Comput Neurosci* 28:361–374. doi:[10.1007/s10827-010-0213-z](https://doi.org/10.1007/s10827-010-0213-z)
- Paolisso G, Scheen AJ, Giugliano D, Sgambato S, Albert A, Varricchio M, D’Onofrio F, Lefévre PJ (1991) Pulsatile insulin delivery has greater metabolic effects than continuous hormone administration in man: Importance of pulse frequency. *J Clin Endocrinol Metab* 72:607–615. doi:[10.1210/jcem-72-3-607](https://doi.org/10.1210/jcem-72-3-607)
- Pinton P, Giorgi C, Siviero R, Zecchini E, Rizzuto R (2008) Calcium and apoptosis: ER-mitochondria  $Ca^{2+}$  transfer in the control of apoptosis. *Oncogene* 27:6407–6418. doi:[10.1038/onc.2008.308](https://doi.org/10.1038/onc.2008.308)

- Polonsky KS, Given BD, Hirsch LJ, Tillil H, Shapiro ET, Beebe C, Frank BH, Galloway JA, Van Cauter E (1988) Abnormal patterns of insulin secretion in non-insulin-dependent diabetes mellitus. *N Engl J Med* 318:1231–1239. doi:[10.1056/NEJM198805123181903](https://doi.org/10.1056/NEJM198805123181903)
- Pørksen N (2002) The in vivo regulation of pulsatile insulin secretion. *Diabetologia* 45:3–20. doi:[10.1007/s125-002-8240-x](https://doi.org/10.1007/s125-002-8240-x)
- Rao A, Luo C, Hogan PG (1997) Transcription factors of the NFAT family: regulation and function. *Annu Rev Immunol* 15:707–747. doi:[10.1146/annurev.immunol.15.1.707](https://doi.org/10.1146/annurev.immunol.15.1.707)
- Ravier M, Sehlin J, Henquin JC (2002) Disorganization of cytoplasmic  $\text{Ca}^{2+}$  oscillations and pulsatile insulin secretion in islets from ob/ob mice. *Diabetologia* 45:1154–1163. doi:[10.1007/s00125-002-0883-9](https://doi.org/10.1007/s00125-002-0883-9)
- Ren J, Sherman A, Bertram R, Goforth PB, Nunemaker CS, Waters CD, Satin LS (2013) Slow oscillations of  $\text{K}_{\text{ATP}}$  conductance in mouse pancreatic islets provide support for electrical bursting driven by metabolic oscillations. *Am J Physiol* 305:E805–E817. doi:[10.1152/ajpendo.00046.2013](https://doi.org/10.1152/ajpendo.00046.2013)
- Rinzel J, Ermentrout GB (1998) Analysis of neural excitability and oscillations. In: Koch C, Segev I (eds) *Methods in neuronal modeling: from synapses to networks*, 2nd edn. MIT Press, Cambridge, pp 251–291
- Robb-Gaspers LD, Burnett P, Rutter GA, Denton RM, Rizzuto R, Thomas AP (1998) Integrating cytosolic calcium signals into mitochondrial metabolic responses. *EMBO J* 17:4987–5000. doi:[10.1093/emboj/17.17.4987](https://doi.org/10.1093/emboj/17.17.4987)
- Rorsman P, Braun M (2013) Regulation of insulin secretion in human pancreatic islets. *Annu Rev Physiol* 75:155–179. doi:[10.1146/annurev-physiol-030212-183754](https://doi.org/10.1146/annurev-physiol-030212-183754)
- Rosati B, McKinnon D (2004) Regulation of ion channel expression. *Circ Res* 94:874–883. doi:[10.1161/01.RES.0000124921.81025.1F](https://doi.org/10.1161/01.RES.0000124921.81025.1F)
- Rosen LB, Ginty DD, Greenberg ME (1995) Calcium regulation of gene expression. *Adv Second Messenger Phosphoprot Res* 30:225–253
- Salazar C, Politi AZ, Hofer T (2008) Decoding of calcium oscillations by phosphorylation cycles: analytic results. *Biophys J* 94:1203–1215. doi:[10.1529/biophysj.107.113084](https://doi.org/10.1529/biophysj.107.113084)
- Santos RM, Rosario LM, Nadal A, Garcia-Sancho J, Soria B, Valdeolmillos M (1991) Widespread synchronous  $\text{Ca}^{2+}$  oscillations due to bursting electrical activity in single pancreatic islets. *Pflügers Arch Eur J Physiol* 418:417–422. doi:[10.1007/BF00550880](https://doi.org/10.1007/BF00550880)
- Schuster S, Knoke B, Marhl M (2005) Differential regulation of proteins by bursting calcium oscillations—a theoretical study. *BioSystems* 81:49–63. doi:[10.1016/j.biosystems.2005.02.004](https://doi.org/10.1016/j.biosystems.2005.02.004)
- Seghers V, Nakazaki M, DeMayo F, Aguilar-Bryan L, Bryan J (2000) Sur1 knockout mice. A model for  $\text{K}_{\text{ATP}}$  channel-independent regulation of insulin secretion. *J Biol Chem* 275:9270–9277. doi:[10.1074/jbc.275.13.9270](https://doi.org/10.1074/jbc.275.13.9270)
- Segil N, Roberts SB, Heintz N (1991) Mitotic phosphorylation of the Oct-1 homeodomain and regulation of Oct-1 DNA binding activity. *Science* 254:1814–1816. doi:[10.1126/science.1684878](https://doi.org/10.1126/science.1684878)
- Shah P, Demirbilek H, Hussain K (2014) Persistent hyperinsulinaemic hypoglycaemia in infancy. *Semin Pediatr Surg* 23:76–82. doi:[10.1053/j.sempedsurg.2014.03.005](https://doi.org/10.1053/j.sempedsurg.2014.03.005)
- Sheng M, Thompson MA, Greenberg ME (1991) CREB: a  $\text{Ca}^{2+}$ -regulated transcription factor phosphorylated by calmodulin-dependent kinases. *Science* 252:1427–1430. doi:[10.1126/science.1646483](https://doi.org/10.1126/science.1646483)
- Sjöholm Å (1995) Regulation of insulinoma cell proliferation and insulin accumulation by peptides and second messengers. *Ups J Med Sci* 100:201–216. doi:[10.3109/03009739509178906](https://doi.org/10.3109/03009739509178906)
- Smedler E, Uhlén P (2014) Frequency decoding of calcium oscillations. *Biochim Biophys Acta Gen Subj* 1840:964–969. doi:[10.1016/j.bbagen.2013.11.015](https://doi.org/10.1016/j.bbagen.2013.11.015)
- Song SH, McIntyre SS, Shah H, D Veldhuis J, Hayes PC, Butler PC (2007) Direct measurement of pulsatile insulin secretion from the portal vein in human subjects. *J Clin Endocrinol Metab* 85:4491–4499. doi:[10.1210/jcem.85.12.7043](https://doi.org/10.1210/jcem.85.12.7043)
- Stemmer PM, Klee CB (1994) Dual calcium ion regulation of calcineurin by calmodulin and calcineurin B. *Biochemistry* 33:6859–6866. doi:[10.1021/bi00188a015](https://doi.org/10.1021/bi00188a015)
- Sturis J, Pugh WL, Tang J, Ostrega DM, Polonsky JS, Polonsky KS (1994) Alterations in pulsatile insulin secretion in the Zucker diabetic fatty rat. *Am J Physiol* 267:E250–E259
- Swulius MT, Waxham MN (2013)  $\text{Ca}^{2+}$ /calmodulin-dependent protein kinases. *Cell Mol Life Sci* 65:2637–2657. doi:[10.1007/s00018-008-8086-2](https://doi.org/10.1007/s00018-008-8086-2)
- Temporal S, Lett KM, Schulz DJ (2014) Activity-dependent feedback regulates correlated ion channel mRNA levels in single identified motor neurons. *Curr Biol* 24:1899–1904. doi:[10.1016/j.cub.2014.06.067](https://doi.org/10.1016/j.cub.2014.06.067)

- Tsien RY, Li W, Llopis J, Whitney M, Zlokarnik G (1998) Cell-permeant caged InsP3 ester shows that  $\text{Ca}^{2+}$  spike frequency can optimize gene expression. *Nature* 392:936–941. doi:[10.1038/31965](https://doi.org/10.1038/31965)
- Turrigiano G, Abbott LF, Marder E (1994) Activity-dependent changes in the intrinsic properties of cultured neurons. *Science* 264:974–977. doi:[10.1126/science.8178157](https://doi.org/10.1126/science.8178157)
- Vigmond EJ, Trayanova NA, Malkin RA (2001) Excitation of a cardiac muscle fiber by extracellularly applied sinusoidal current. *J Cardiovasc Electrophysiol* 12:1145–1153. doi:[10.1097/FJC.0b013e3181a25078.CaMKII](https://doi.org/10.1097/FJC.0b013e3181a25078.CaMKII)
- Wang Z, Zhou Y, Luo Y, Zhang J, Zhai Y, Yang D, Zhang Z, Li Y, Storm DR, Ma RZ (2015) Gene expression profiles of main olfactory epithelium in adenylyl cyclase 3 knockout mice. *Int J Mol Sci* 16:28320–28333. doi:[10.3390/ijms161226107](https://doi.org/10.3390/ijms161226107)
- West AE, Chen WG, Dalva MB, Dolmetsch RE, Kornhauser JM, Shaywitz AJ, Takasu MA, Tao X, Greenberg ME (2001) Calcium regulation of neuronal gene expression. *Proc Natl Acad Sci* 98:11024–11031. doi:[10.1073/pnas.191352298](https://doi.org/10.1073/pnas.191352298)
- Wu Z, Xing J (2012) Functional roles of slow enzyme conformational changes in network dynamics. *Biophys J* 103:1052–1059. doi:[10.1016/j.bpj.2012.08.008](https://doi.org/10.1016/j.bpj.2012.08.008)
- Xu M, Welling A, Papparisto S, Hofmann F, Klugbauer N (2003) Enhanced expression of L-type  $\text{Ca}_v$ 1.3 calcium channels in murine embryonic hearts from  $\text{Ca}_v$ 1.2-deficient mice. *J Biol Chem* 278:40837–40841. doi:[10.1074/jbc.M307598200](https://doi.org/10.1074/jbc.M307598200)
- Zhang M, Goforth P, Sherman A, Bertram R, Satin LS (2003) The  $\text{Ca}^{2+}$  dynamics of isolated mouse  $\beta$ -cells and islets: implications for mathematical models. *Biophys J* 84:2852–2870. doi:[10.1016/S0006-3495\(03\)70014-9](https://doi.org/10.1016/S0006-3495(03)70014-9)
- Zhang Q, Bhattacharya S, Andersen ME (2013) Ultrasensitive response motifs: basic amplifiers in molecular signalling networks. *Open Biol* 3:130031. doi:[10.1098/rsob.130031](https://doi.org/10.1098/rsob.130031)
- Zhou J, Kodirov S, Murata M, Miao S, Zheng J, Zhang C, Xiong ZQ (2003) Regional upregulation of Kv2.1-encoded current,  $\text{I}_{K,\text{slow}2}$ , in Kv1DN mice is abolished by crossbreeding with Kv2DN mice. *Am J Physiol* 284:H491–H500. doi:[10.1152/ajpheart.00576.2002](https://doi.org/10.1152/ajpheart.00576.2002)
- Zhu L, Luo Y, Chen T, Chen F, Wang T, Hu Q (2008)  $\text{Ca}^{2+}$  oscillation frequency regulates agonist-stimulated gene expression in vascular endothelial cells. *J Cell Sci* 121:2511–2518. doi:[10.1242/jcs.031997](https://doi.org/10.1242/jcs.031997)